3 RESULTS AND DISCUSSIONS

Gas Chromatography (GC) has been widely used for amine analysis because of it inherent advantage of simplicity, high resolving power, high sensitivity, short analysis time and low cost. However, the GC of free amines, without special modification to the column, is unsatisfactory owing to the adsorption and decomposition of the solute, resulting in peak tailing and losses. (Kataoka, 1996).

Derivatization is one of a popular method for overcoming the above problems. It has been employed to reduce the polarity of the amino group and to improve GC properties. Derivatization reactions, often selective for amine type, have also been used to improve the detection and separation of these amines. Many derivatization reagents for GC analyses of amines such as trifluoroacetic and heptafluorobutyric anhydrides, pentafluorobenzylbromide (PFB-BRr), 3,5-bistrifluoromethylbenzylbromide(bis-TFMBZ-Br) and bis trifluoromethylbenzoyl bromide (bis-TFMBO-Cl) have been tested as derivatization reagents for some HCAs. However, acylation with acid anhydride gave very poor GC properties (Kataoka *et al.*, 1997). Although the alkylation products with PFB-Br, bis–TFMBZ-Br and bis-TFMBO-Cl had good GC properties for some HCAs, these methods gave a mixture of mono– and di-alkylated forms. Incompleted derivatization leads to non-reproducible results (Kataoka *et al.*, 1997).Consequently, a useful GC method has not yet been developed.

This research work investigated a convenient and reliable method for the simultaneous determination of HCAs by the GC with nitrogen-phosphorus selective detector after simple derivatization with N, N-dimethylformamide dimethyl acetal (DMF-DMA), derivatizing reagent. It has been used not only to react with methyl esterification of carboxylic acid but also for a one-step derivatization of amino acids into N, N-dimethylaminomethylene methyl

esters. The reaction with amino group is based on Schiff base condensation of primary amines. Therefore, it is considered that each HCA gives a single derivative by the reaction with DMF-DFA. Figures 10-12 show Schiff base type reactions of HCAs

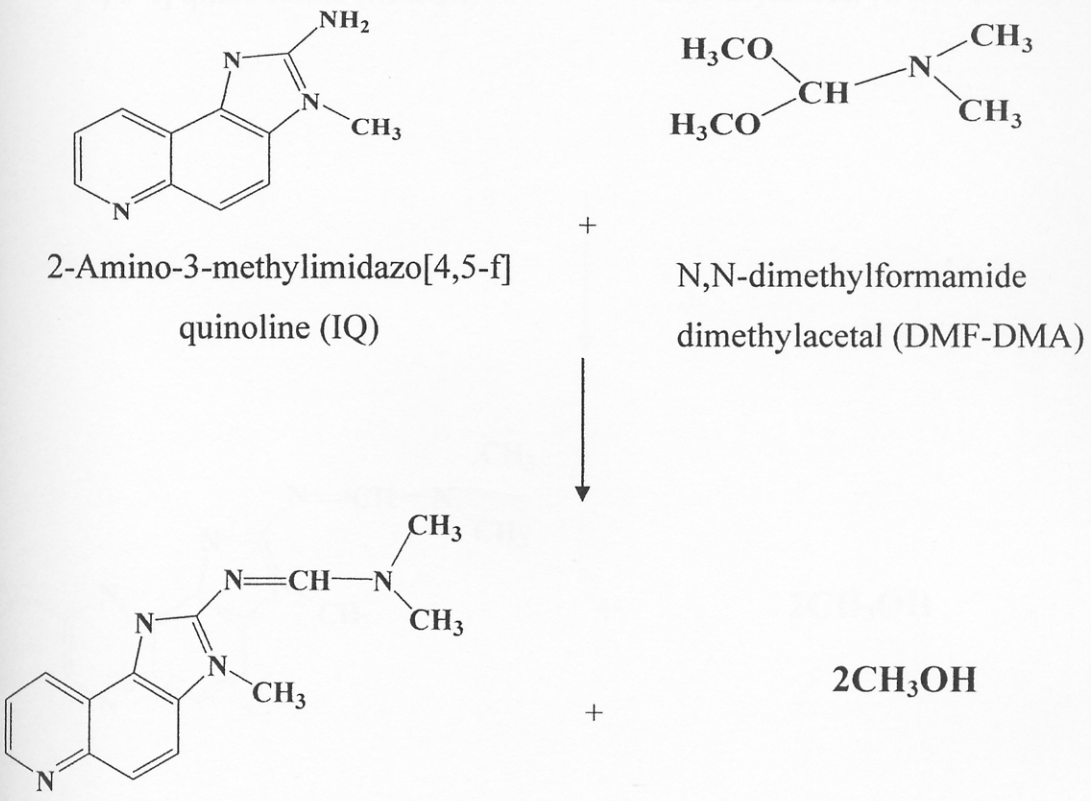

N, N-dimethylaminomethylene derivative of IQ

Figure 10 Schiff base reaction of IQ

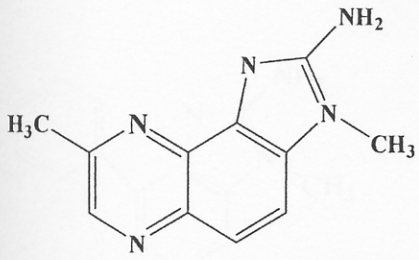

2-Amino-3, 8-dimethylimidazo
[4, 5-f] quinoxaline (MeIQx)

+

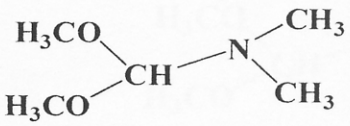

N, N-dimethylformamide
dimethylacetal (DMF-DMA)

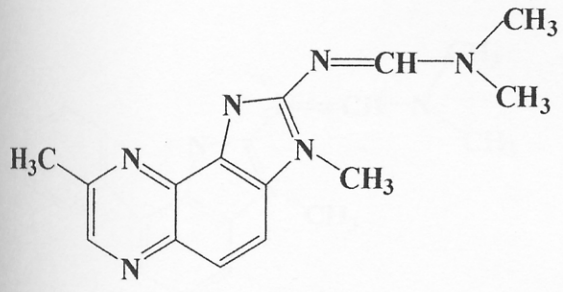

+ **2CH$_3$OH**

N, N-dimethylaminomethylene derivative of MeIQx

Figure 11 Schiff base reaction of MeIQx

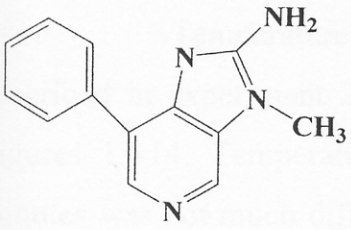

+

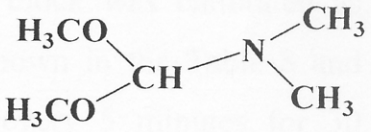

2-Amino-1-methyl-6-phenylimidazo [4, 5-b]pyridine (PhIP)

N, N-dimethylformamide dimethylacetal (DMF-DMA)

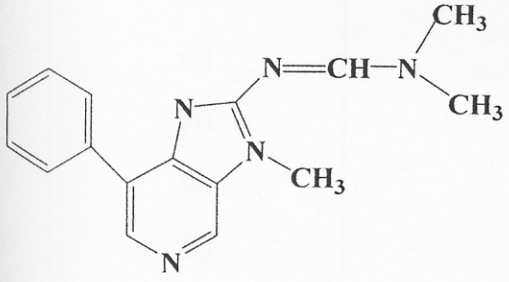

+ **2CH$_3$OH**

N, N-dimethylaminomethylene derivative of PhIP

Figure 12 Schiff base reaction of PhIP

3.1 Optimization of the derivatization reaction

3.1.1 Calibration of the temperature for the lab-built heating unit

Temperature of the lab built heating block was calibrated as described in experiment 2.4.1 and the results are shown in the Table 8 and Figures 13-14. Temperature read from the meter every 5 minutes for 30 minutes was not much different from the set temperature of the heating block, with percentage RSD of less than 1%. That is the lab built heating block can control the heat required for derivatization reaction.

Table 8 The relationship between the set temperature and the actual temperature of the lab built heating block

Set temperature (°C)	Temperature read every 5 minutes for 30 minutes (°C) * (± SD)
50	50.6 ± 0.2
60	60.1 ± 0.2
70	70.1 ± 0.1
80	80.8 ± 0.1
90	90.2 ± 0.1
100	100.1± 0.1
110	110.5 ± 0.1
120	120.6 ± 0.3
130	130.4 ± 0.2
140	140.4 ± 0.3
150	150.7 ± 0.1

*5 replications after reached actual temperature

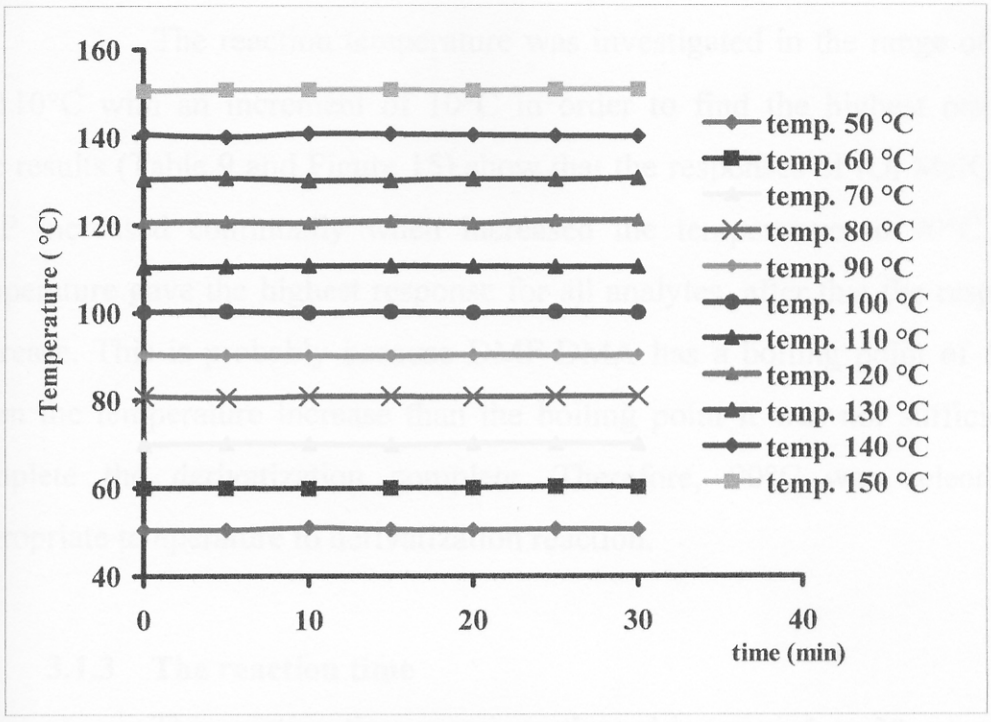

Figure 13 Temperature read from every 5 minutes

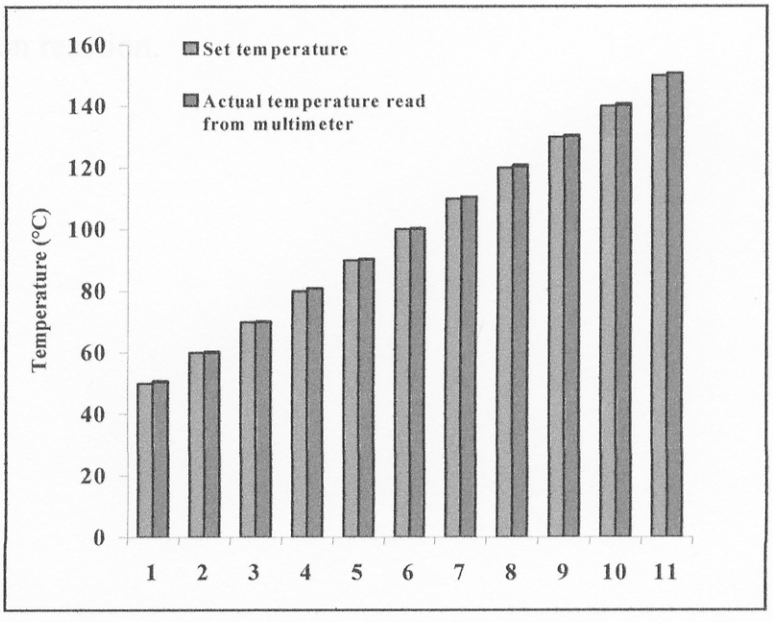

Figure 14 The relationship between the set temperature and the measured temperature

3.1.2 The reaction temperature

The reaction temperature was investigated in the range of 70°C to 110°C with an increment of 10°C in order to find the highest response. The results (Table 9 and Figure 15) show that the responses of IQ, MeIQx and PhIP increased continually when increased the temperature to 90°C. This temperature gave the highest response for all analytes, after that the responses decrease. This is probably because DMF-DMA has a boiling point of 108°C when the temperature increase than the boiling point it was not sufficient to complete the derivatization complete. Therefore, 90°C was selected as appropriate temperature to derivatization reaction.

3.1.3 The reaction time

The reaction time was investigated between 5 to 30 minutes to find the highest response. The results obtained from experiment 2.4.5.2 are shown in Table 10 and Figure 16. The reaction time at 10 minutes provided the highest response and this was selected as the optimum reaction time for derivatization reaction.

Table 9 The responses of three HCA derivatives standard solution of reaction temperature on the conversion of HCAs into their N-dimethylaminomethylene derivatives

Reaction temperature (°C)	Response* × 10^4 (μV) ± SD		
	IQ	MeIQx	PhIP
70	98.6 ± 0.4	13.6 ± 0.2	13.4 ± 1.2
80	98.3 ± 0.1	18.0 ± 0.7	16.8 ± 0.1
90	99.1 ± 0.7	23.4 ± 0.6	19.8 ± 0.6
100	98.0 ± 0.2	20.9 ± 0.4	19.6 ± 0.4
110	38.0 ± 1.0	5.6 ± 0.2	5.4 ± 0.2

* 5 replications, RSD < 4%

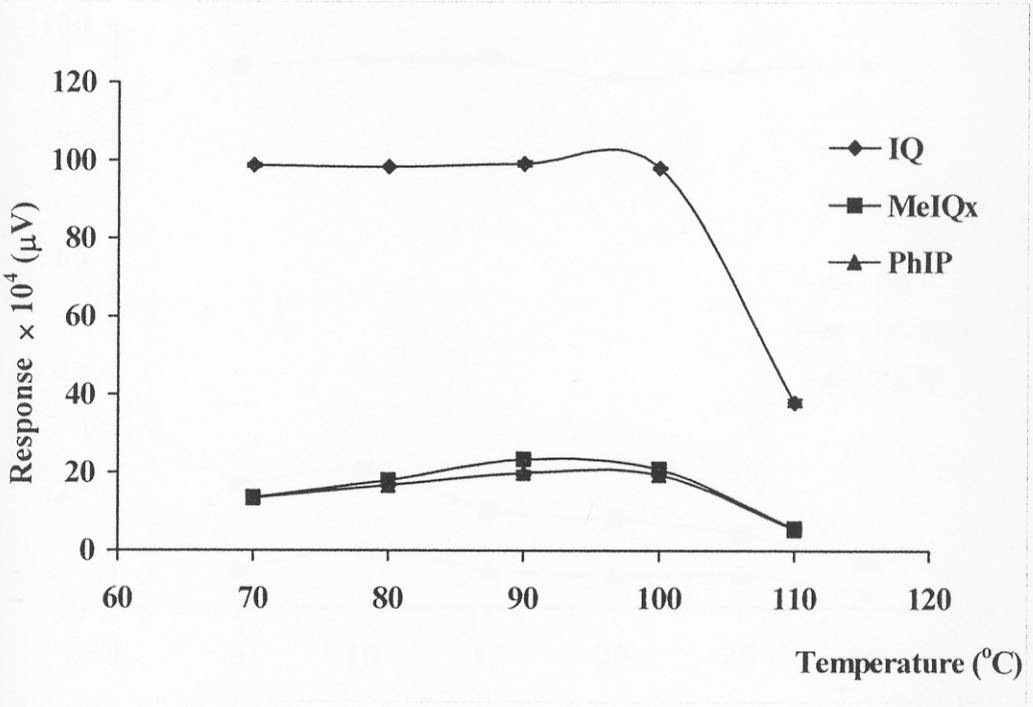

Figure 15 The responses of three HCA derivatives standard solution of reaction temperature on the conversion of HCAs into their N-dimethylaminomethylene derivatives

Table 10 Responses of three N-dimethylaminomethylene HCA derivatives with various reaction times

Reaction time (minutes)	Response* × 10^4 (μV) ± SD		
	IQ	MeIQx	PhIP
5	92.7 ± 1.2	21.2 ± 0.8	6.6 ± 0.2
10	93.9 ± 0.4	23.5 ± 0.2	10.1 ± 0.4
15	93.8 ± 0.9	16.7 ± 0.3	6.4 ± 0.2
20	90.6 ± 0.6	15.1 ± 0.3	5.5 ± 0.2
25	92.3 ± 0.4	12.8 ± 0.4	5.5 ± 0.2
30	92.9 ± 1.0	7.6 ± 0.2	2.6 ± 0.1

* 5 replications, RSD < 4%

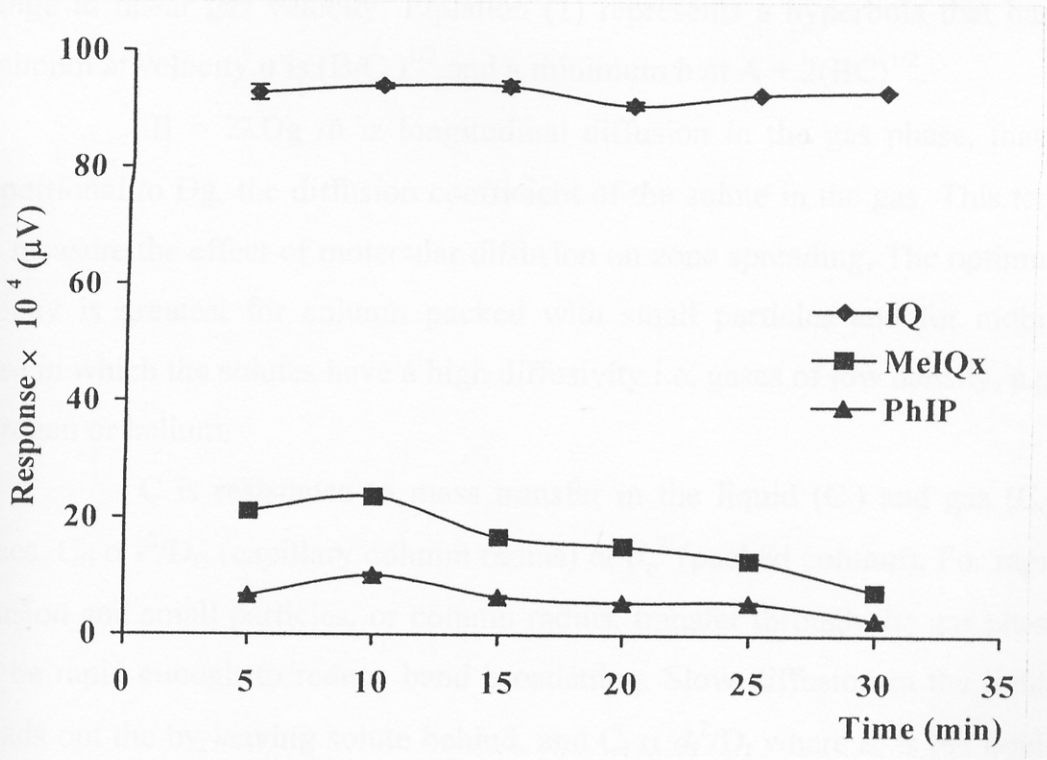

Figure 16 Responses of three N-dimethylaminomethylene HCA derivatives with various reaction times

3.2 Optimization of the GC-NPD conditions for HCAs analysis

3.2.1 The carrier gas flow rate

The carrier gas (helium) flow rate was optimized in experiment 2.4.6.1 by considering the relationship between the height equivalent to a theoretical plate (HETP) and the carrier gas flow rate. The van Deemter equation (equation 1) is used for describing the gas chromatographic process (Townshend, 1995).

$$HETP = A + \frac{B}{\bar{u}} + C_l \bar{u} + C_g \bar{u} \qquad (1)$$

Where

$A = 2\lambda dp$ is eddy diffusion term, λ is the packing uniformity, and dp is the particle diameter. The eddy diffusion shows the effect of h with change in linear gas velocity. Equation (1) represents a hyperbola that has a minimum at velocity u is $(B/C)^{1/2}$ and a minimum h at $A + 2(BC)^{1/2}$.

$B = 2\lambda Dg / \bar{u}$ is longitudinal diffusion in the gas phase, that is proportional to Dg, the diffusion coefficient of the solute in the gas. This term is a measure the effect of molecular diffusion on zone spreading. The optimum velocity is greatest for column packed with small particles and for mobile phase in which the solutes have a high diffusivity i.e. gases of low density, e.g., hydrogen or helium.

C is resistance to mass transfer in the liquid (C_l) and gas (C_G) phases. $C_G \alpha r^2/D_G$ (capillary column radius) or d_p^2 (packed column). For rapid diffusion and small particles, or column radius, transfer through the gas phase will be rapid enough to reduce band broadening. Slow diffusion in the liquid spreads out the by leaving solute behind, and $C_l \alpha d_f^2/D_l$ where d_f is the liquid film thickness and D_l is the diffusion coefficient for the solute in the liquid.

The relative magnitude of the different term in Equation (1) for GC are shown in Figure 17. A low $\bar{u}$, the B term is large, but quickly

diminishes with increasing ū and C_G to a lesser extent, C_l, then dominate.The smallest value of H is H_{min}, at with ū is optimum, $ū_{opt}$. The greater $ū_{opt}$, the faster a sample can be analyzed. (Bartle, 1993).

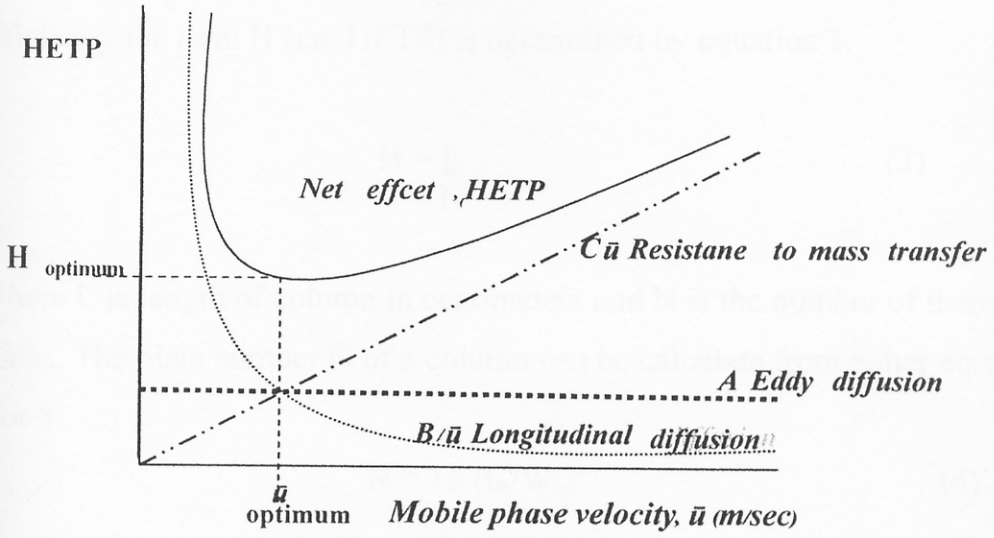

Figure 17 Relative magnitudes of the different terms in the van Deemter equation

In this research, a 30 m × 0.25 mm I.D., narrow bore wall–coated open tubular (WCOT) column or capillary column was used for the analysis. In this column a liquid phase is coated on fused silica wall with no packing material, no eddy diffusion, therefore, the equation contains only two terms. The A term is nonexistent because there is only one flow path and no packing material. The resistance-to-mass-transfer term C has the greatest effect on band broadening, and its effect in capillary columns is controlled by the mass transfer in the gas phase. Equation (1) takes a different form for capillary columns.

$$HETP = \frac{B}{ū} + C_G ū \qquad (2)$$

which is known as the Golay equation (Townshend, 1995).

The above equation showed that HETP is proportional to the flow rate of carrier gas (ū). It is also known that an optimum carrier gas flow rate reflected the high number of theoretical plates *i.e.* the high column efficiency and high resolution where at the lowest HETP (Grob, 1985). The indication of column efficiency the term H (*i.e.* HETP) is determined by equation 3.

$$H = \frac{L}{N} \qquad (3)$$

Where L is length of column in centimeters and N is the number of theoretical plates. The plate number N of a column can be calculate from either equation 4 or 5.

$$N = 16\ (t_R/W_b)^2 \qquad (4)$$

or

$$N = 5.54\ (t_R/W_b)^2 \qquad (5)$$

Since a capillary column was used in this work, sharp peaks were obtained. Therefore, the plate number N could calculated directly from the value obtained from a chromatogram as shown in the Figure 18 and the equation 6 (Grob, 1985)

$$N = 2\pi(t_R h/A)^2 \qquad (6)$$

Where:

t_R is the retention time

A is integrated the peak area

h is integrated peak height

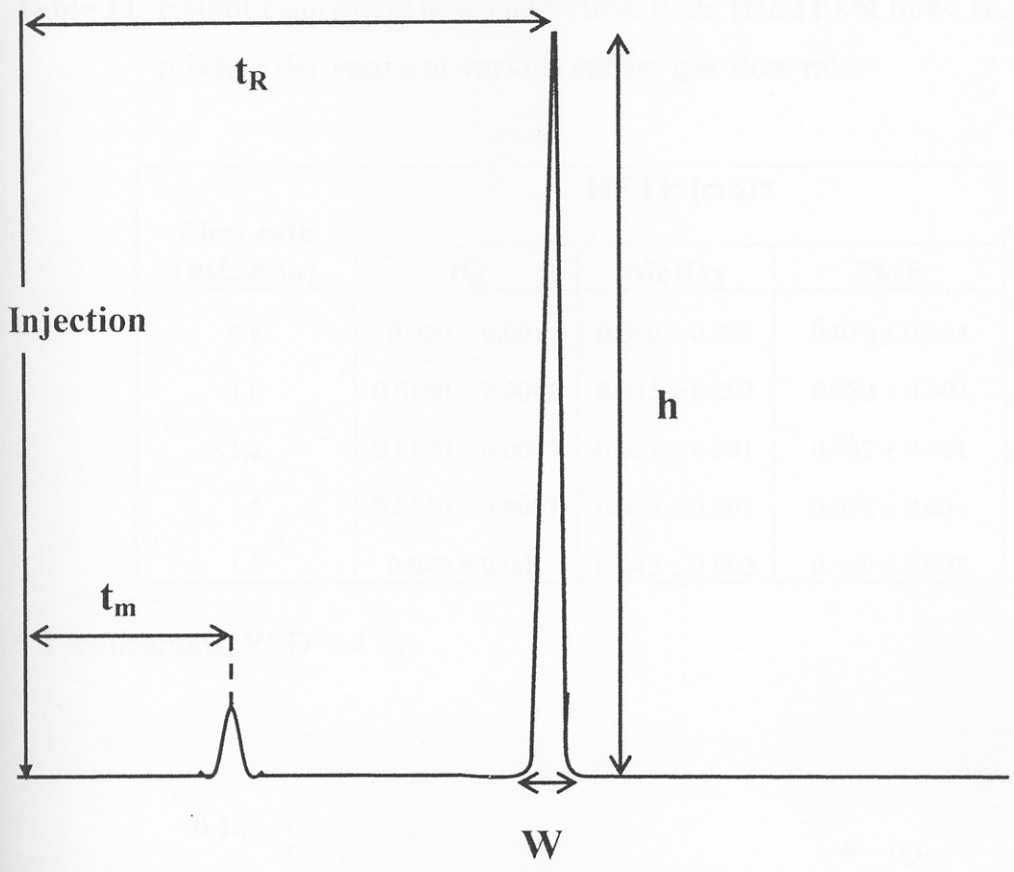

Figure 18 Capillary Chromatogram for calculating the theoretical plates

N was calculated from equation (6) and substituted in equation (3), with a known L, column length, to obtain HETP. The HETP and the carrier gas flow rate plotted, the van Deemter graph (Table 11 and Figure19). From the van Deemter plot, the optimum flow rate was obtained at the narrowest HETP at the carrier gas flow rate of 1.5 mL min^{-1} for all three heterocyclic amine derivatives.

Table 11 Height Equivalent to a Theoretical Plate (HETP) of three HCA mixture derivative at various carrier gas flow rate

Flow rate (mL/min)	HETP (cm)*		
	IQ	MeIQx	PhIP
0.8	0.020 ± 0.001	0.060 ± 0.001	0.070 ± 0.003
1.0	0.0180 ± 0.0002	0.055 ± 0.002	0.080 ± 0.002
1.2	0.0190 ± 0.0005	0.033 ± 0.001	0.032 ± 0.001
1.5	0.0150 ± 0.0003	0.020 ± 0.001	0.028 ± 0.001
1.8	0.040 ± 0.001	0.045 ± 0.002	0.050 ± 0.002

* 5 replications, RSD < 4 %

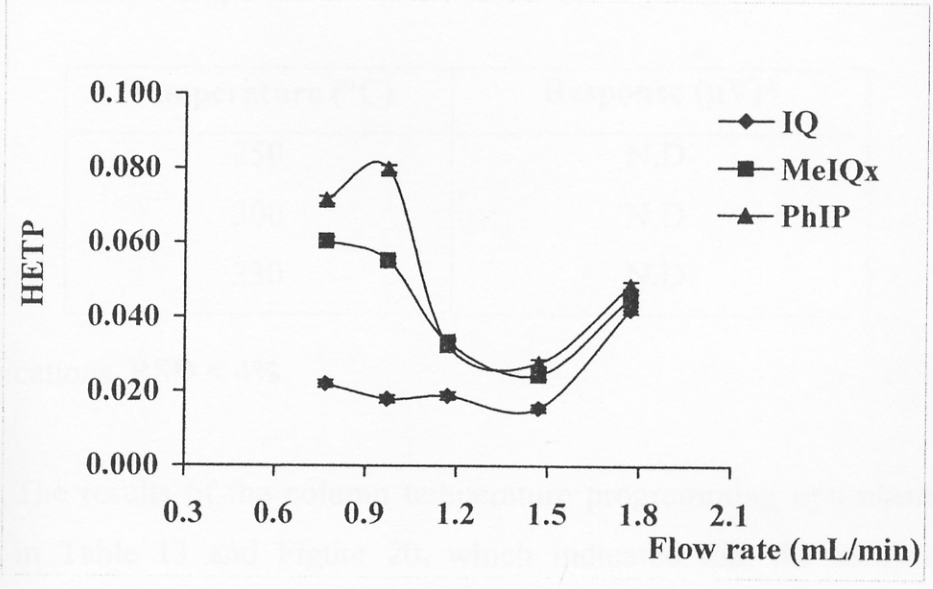

Figure 19 The van Deemter plot of three HCA derivatives

3.2.2 The column temperature programming

The column temperature is one of the important parameter in gas chromatography technique. Initially only the isothermal temperature was optimized, but the result showed poor separation as shown in Table 12. That is the isothermal temperature was not sufficient to elute all the analytes from the GC column. Therefore, the column temperature programming was applied and optimized. The temperature program was used to minimize the time for eluting or separating the components of interest while narrowing peak width and integrating detectability, increasing, sample throughput, and reducing analysis time.

Table 12 The responses of three HCA derivatives mixture on the isothermal column temperatures

Temperature (°C)	Response (μV)*
250	N.D.
300	N.D.
330	N.D.

*5 replications, RSD < 4%

The results of the column temperature programming optimization are shown in Table 13 and Figure 20, which indicated that the analysis time decreased when the temperature increased. The initial temperature at 190°C provides the highest response and a good separation. Therefore, 190°C was chosen for the initial temperature.

Table 14 and Figure 21 showed the responses of HCA derivatives at different hold time of initial temperature. The responses increased as with the hold time increased from 0 to 3 minutes and after 3 minutes the responses

leveled off. Thus, the hold time of 3 minutes was chosen as the optimum hold time.

Table 13 The responses of three HCA derivatives at various initial temperatures

Intitial Temperature (°C)	Response* × 10^4 (μV) ± SD		
	IQ	MeIQx	PhIP
150	99.2 ± 0.3	7.4 ± 0.3	5.7 ± 0.2
160	97.3 ± 0.2	7.8 ± 0.2	5.6 ± 0.2
170	99.1 ± 0.5	8.7 ± 0.4	5.9 ± 0.2
180	98.5 ± 2.6	13.3 ± 0.5	9.0 ± 0.3
190	98.2 ± 1.0	14.5 ± 0.5	9.9 ± 0.3
200	89.2 ± 2.8	7.8 ± 0.1	6.5 ± 0.1
210	76.2 ± 2.2	7.8 ± 0.1	6.6 ± 0.1

* 5 replications, RSD < 4%

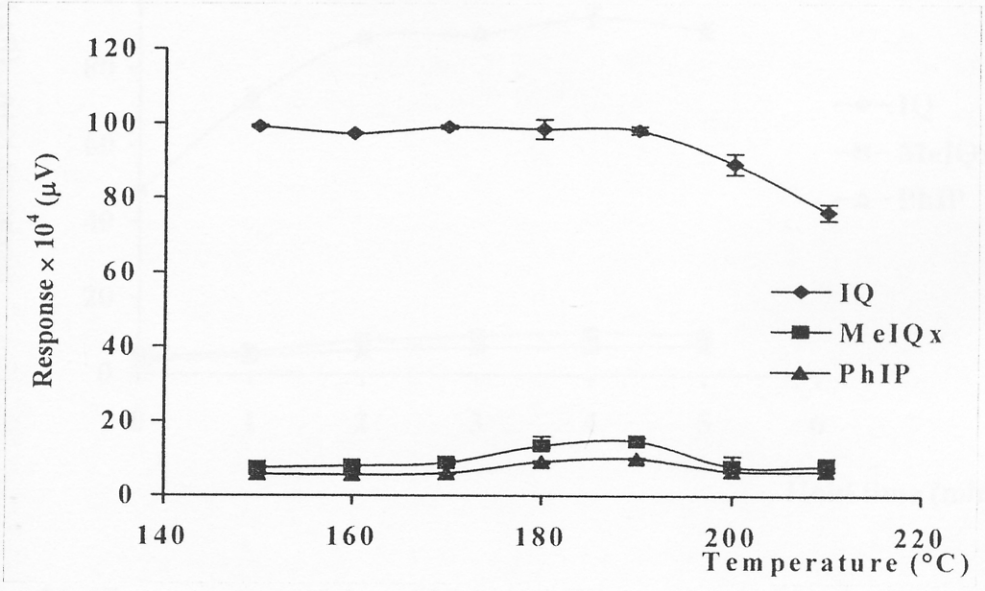

Figure 20 The responses of three HCA derivatives at various initial temperatures

Table 14 The responses of three HCA derivatives at various hold times

Hold time at initial temperature (minutes)	Response* × 10^4 (μV) ± SD		
	IQ	MeIQx	PhIP
0	47.8 ± 1.4	4.4 ± 0.1	3.4 ± 0.1
1	72.2 ± 2.4	6.0 ± 0.2	4.8 ± 0.1
2	88.0 ± 1.0	8.9 ± 0.3	6.5 ± 0.2
3	89.1 ± 1.3	10.0 ± 0.2	7.1 ± 0.2
4	93.5 ± 2.7	11.0 ± 0.4	7.4 ± 0.1
5	90.3 ± 2.2	10.7 ± 0.2	7.6 ± 0.4

*5 replications, RSD < 4%

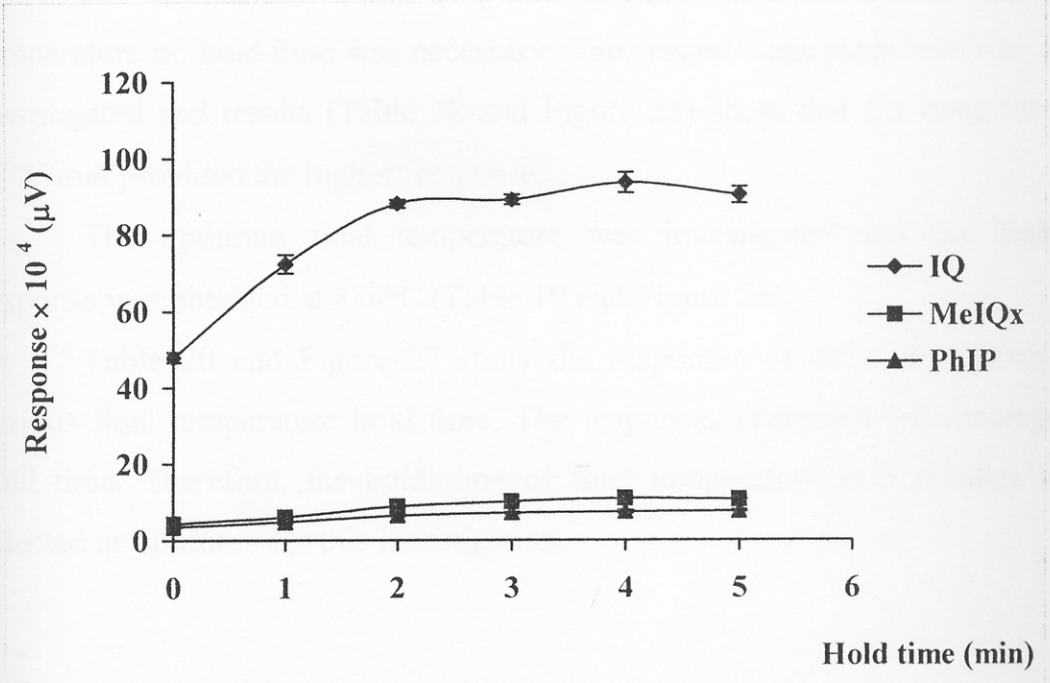

Figure 21 The responses of three HCA derivatives at various hold times

After holding the temperature at 190°C for 3 minutes, the column temperature was programmed to increase rapidly to 300°C with various ramp rates. Table 15 and Figure 22 showed the results of various ramp rates. The ramp rate at 35°C/min provided the highest response. Thus, the optimum ramp rate of 35°C/min was selected.

The column temperature at the second stage was investigated from 250°C to 290°C. The results are shown in Table 16 and Figure 23. The highest response was found at 280°C and this was selected to be the optimum of second stage of temperature.

Table 17 and Figure 24 showed the responses of three HCA derivatives at various hold time at the second stage of temperature at 280°C. The responses decreased when increased the hold time. Therefore, at this second stage of temperature no hold time was necessary. The second stage ramp rate was also investigated and results (Table 18 and Figure 25) show that the ramp rate at 10°C/min provided the highest response.

The optimum final temperature was investigated and the highest response was obtained at 330°C (Table 19 and Figure 26).

Table 20 and Figure 27 show the responses of HCA derivatives at various final temperature hold time. The responses decreased with increased hold time. Therefore, the hold time of final temperature at 5 minutes was selected as optimum for this investigation.

Table 15 The responses of HCA derivatives at various ramp rates for first stage

Ramp rate (°C/min)	Response* × 10^4 (μV) ± SD		
	IQ	MeIQx	PhIP
10	43.6± 1.1	3.3 ± 0.1	2.4 ± 0.1
20	46.5± 1.4	4.8 ± 0.1	3.1 ± 0.1
30	52.4 ± 1.8	6.2 ± 0.2	3.9 ± 0.1
35	66.7 ± 2.2	7.1 ± 0.3	4.2 ± 0.1
40	49.5 ± 2.0	5.8 ± 0.2	3.5 ± 0.1

*5 replications, RSD < 4%

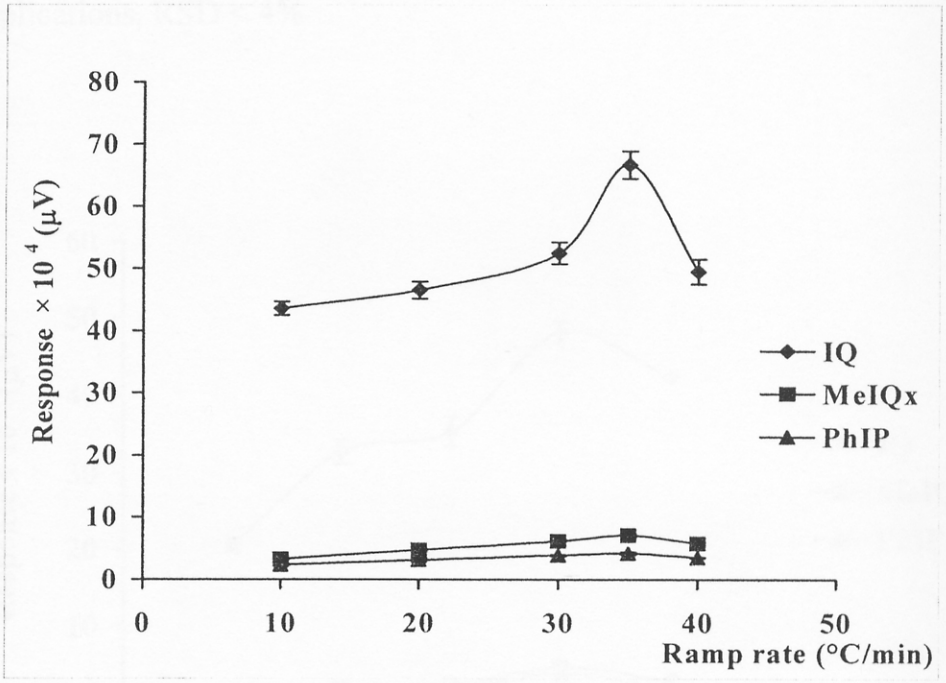

Figure 22 The responses of HCA derivatives at various ramp rates for first stage

Table 16 The responses of HCA derivatives at various column temperatures at second stage

Second stage of temperature (°C)	Response* × 10^4 (μV) ±SD		
	IQ	MeIQx	PhIP
250	20.5 ± 0.8	0.54 ± 0.01	0.23 ± 0.01
260	32.6 ± 1.2	2.0 ± 0.1	1.5 ± 0.1
270	35.1 ± 1.4	2.1 ± 0.1	1.45 ± 0.04
280	48.0 ± 1.4	4.5 ± 0.1	3.8 ± 0.2
290	42.0 ± 0.3	2.7 ± 0.1	1.64 ± 0.05

* 5 replications, RSD < 4%

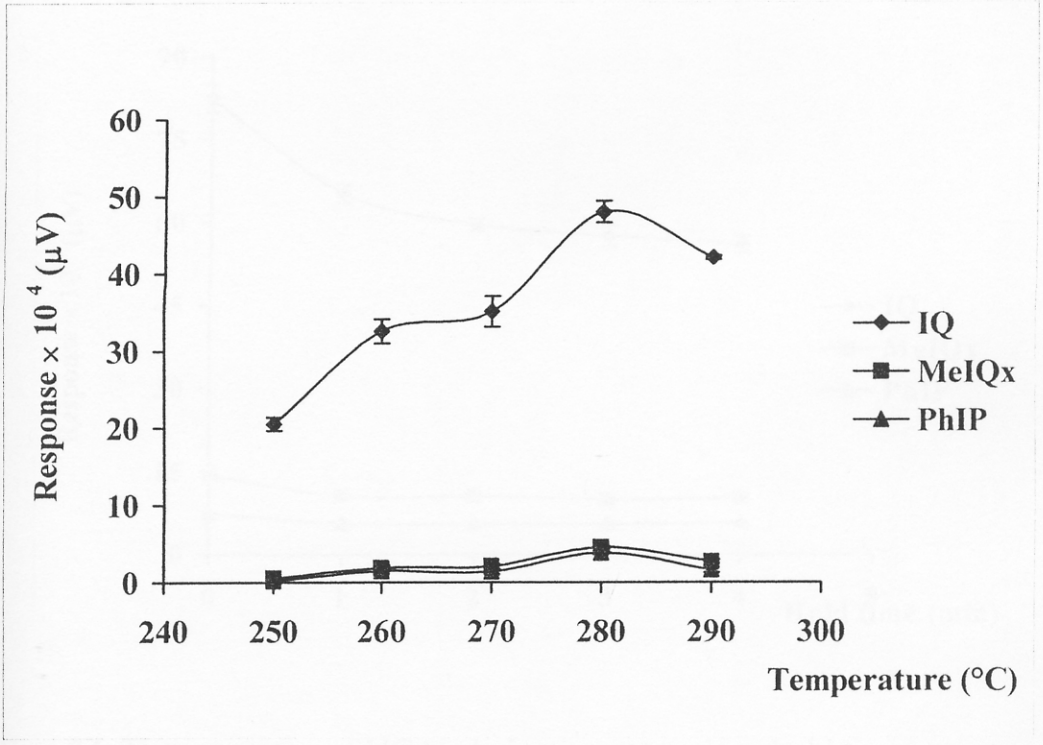

Figure 23 The responses of HCA derivatives at various column temperatures at second stage

Table 17 The responses of HCA derivatives at various hold times at second stage

Hold time at second stage (min)	Response* × 10^4 (μV) ± SD		
	IQ	MeIQx	PhIP
0	82.4 ± 2.4	14.2 ± 0.4	7.3 ± 0.2
1	65.2 ± 1.6	10.6 ± 0.2	5.5 ± 0.2
2	59.7 ± 1.1	10.5 ± 0.2	5.4 ± 0.1
3	57.6 ± 2.0	10.0 ± 0.3	5.4 ± 0.2
4	56.0 ± 1.5	10.3 ± 0.2	5.81 ± 0.04

* 5 replications, RSD < 4%

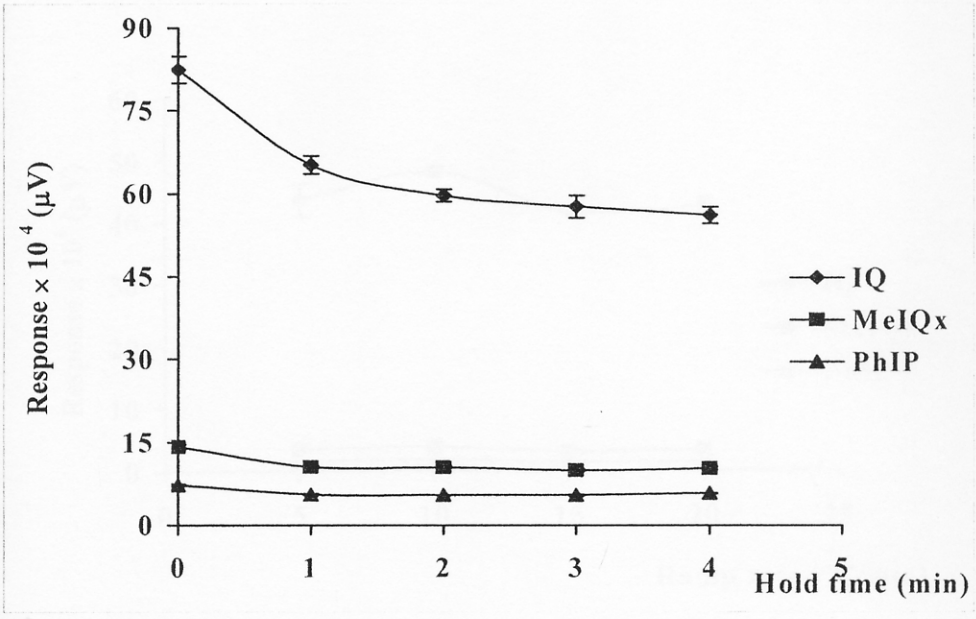

Figure 24 The responses of HCAs derivatives at various hold times at second stage

Table 18 The responses of HCA derivatives at various ramp rates at second stage

Ramp rate at second stage (°C/min)	Response* × 10^4 (μV) ± SD		
	IQ	MeIQx	PhIP
5	43.7 ± 0.2	3.4 ± 0.1	1.63 ± 0.04
10	48.2 ± 0.1	4.0 ± 0.1	1.92 ± 0.07
15	41.8 ± 0.1	3.1 ± 0.1	1.50 ± 0.03
20	42.6 ± 1.4	3.4 ± 0.1	1.50 ± 0.02

* 5 replications, RSD < 4%

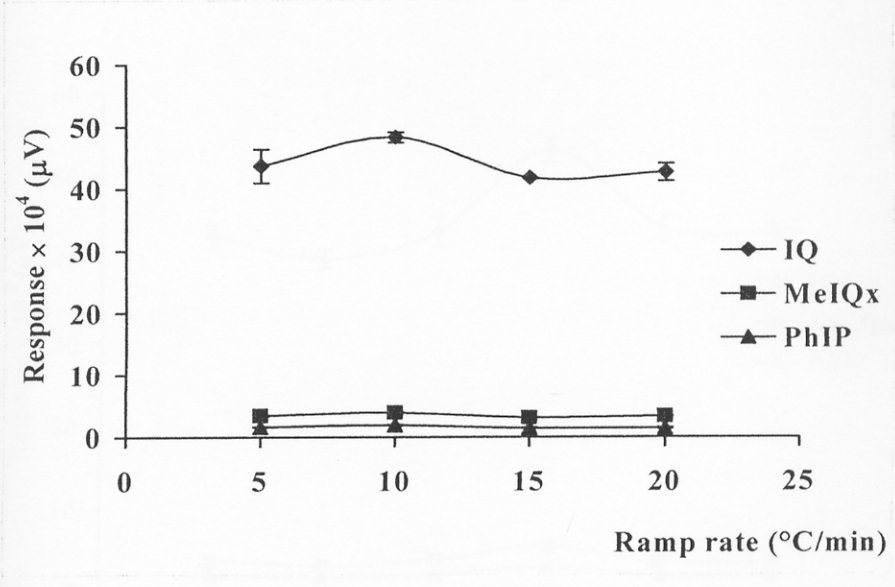

Figure 25 The responses of HCA derivatives at various ramp rates at second stage

Table 19 The responses of HCA derivatives at various column temperatures at the final stage

Final temperature (°C)	Response* × 10^4 (μV) ± SD		
	IQ	MeIQx	PhIP
315	43.0 ± 1.4	3.9 ± 0.2	2.2 ± 0.1
320	40.2 ± 1.1	3.3 ± 0.1	1.90 ± 0.04
325	43.5 ± 1.8	4.1 ± 0.1	2.2 ± 0.1
330	53.5 ± 1.5	5.8 ± 0.2	3.4 ± 0.1
335	44.1 ± 1.8	3.9 ± 0.1	2.3 ± 0.1
340	43.5 ± 1.4	4.0 ± 0.1	2.5 ± 0.1

*5 replications, RSD < 4%

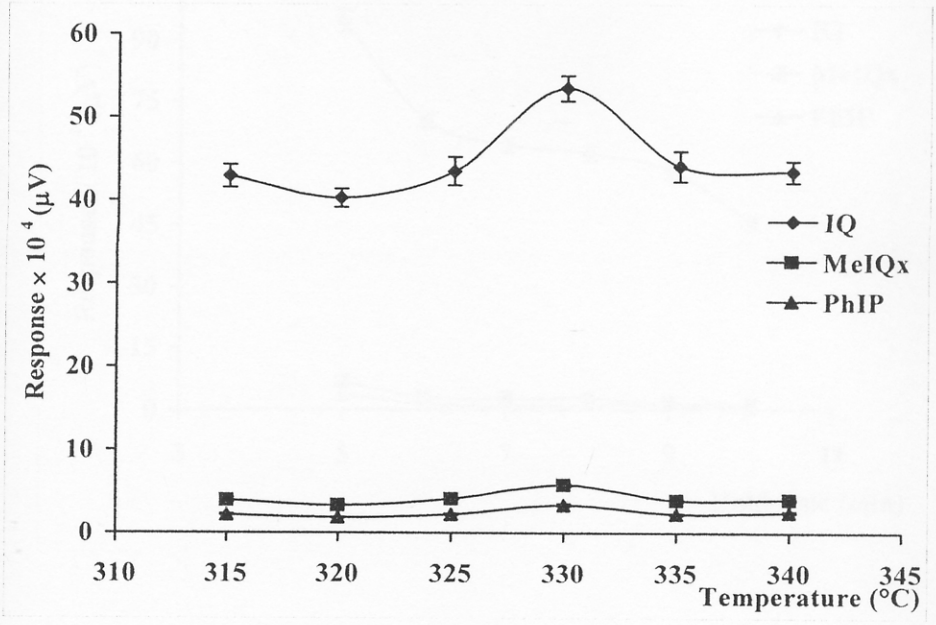

Figure 26 The responses of HCA derivatives at various column temperatures at final stage

Table 20 The responses of HCA derivatives at various hold times at final temperature

Hold time at final temperature (minutes)	Response* $\times 10^4$ (μV) $\pm$ SD		
	IQ	MeIQx	PhIP
5	94.5 $\pm$ 2.8	6.8 $\pm$ 0.2	3.6 $\pm$ 0.2
6	70.2 $\pm$ 1.9	3.0 $\pm$ 0.1	1.30 $\pm$ 0.03
7	64.3 $\pm$ 1.8	2.5 $\pm$ 0.1	1.01$\pm$ 0.04
8	62.3 $\pm$ 2.0	2.8 $\pm$ 0.1	1.11 $\pm$ 0.02
9	58.1 $\pm$ 1.9	1.6 $\pm$ 0.1	1.25 $\pm$ 0.04
10	45.3 $\pm$ 1.6	1.10 $\pm$ 0.02	0.44 $\pm$ 0.01

* 5 replications, RSD < 4%

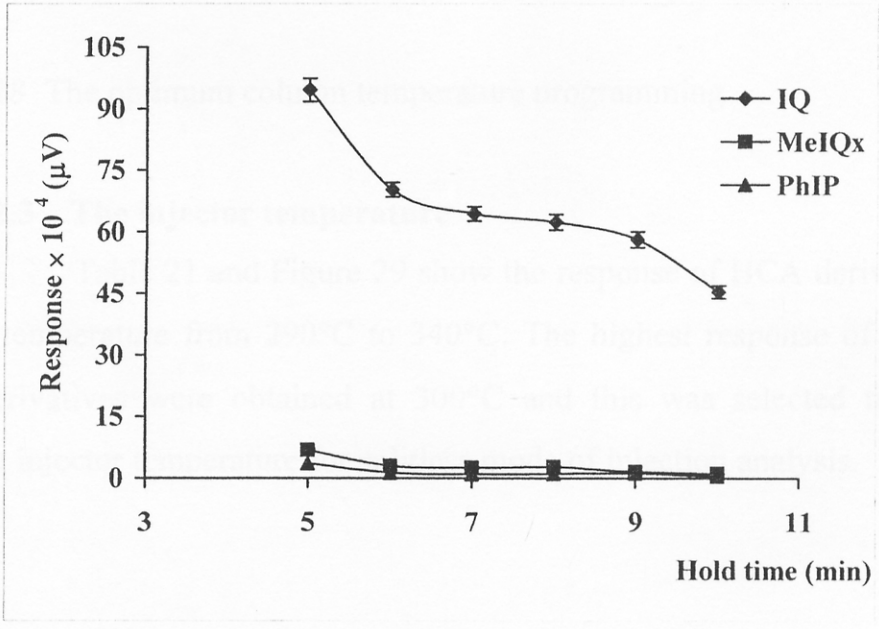

Figure 27 The responses of HCA derivatives at various hold times at final temperature

In summary, the optimum conditions of the column temperature program applied for GC–NPD (Figure 28) was the initial temperature 190°C, hold for 3 minutes, ramped at 35°C/min to 280°C and then ramped at 10°C/min to final temperature 330°C and hold for 5 minutes.

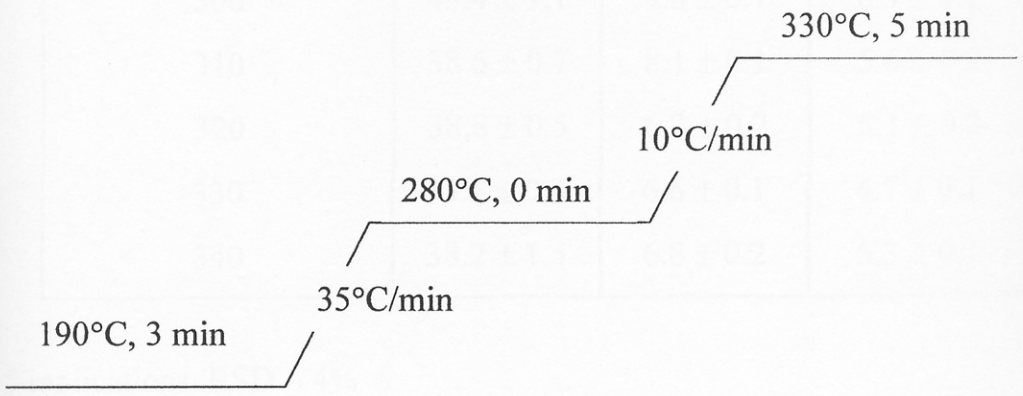

Figure 28 The optimum column temperature programming

3.2.3 The injector temperature

Table 21 and Figure 29 show the response of HCA derivatives at injector temperature from 290°C to 340°C. The highest response of all three HCA derivatives were obtained at 300°C and this was selected to be the optimum injector temperature for splitless mode of injection analysis.

Table 21 The responses of HCA derivatives at various injector temperatures

Injector temperature (°C)	Response* × 10^4 (μV) ± SD		
	IQ	MeIQx	PhIP
290	39.4 ± 0.9	8.1 ± 0.2	5.5 ± 0.2
300	45.4 ± 1.1	9.8 ± 0.1	6.9 ± 0.2
310	38.6 ± 0.7	8.1 ± 0.1	5.6 ± 0.2
320	38.8 ± 0.5	6.2 ± 0.2	5.1 ± 0.2
330	33.5 ± 0.3	6.6 ± 0.1	4.7 ± 0.1
340	38.2 ± 1.5	6.8 ± 0.2	5.3 ± 0.1

* 5 replications, RSD < 4%

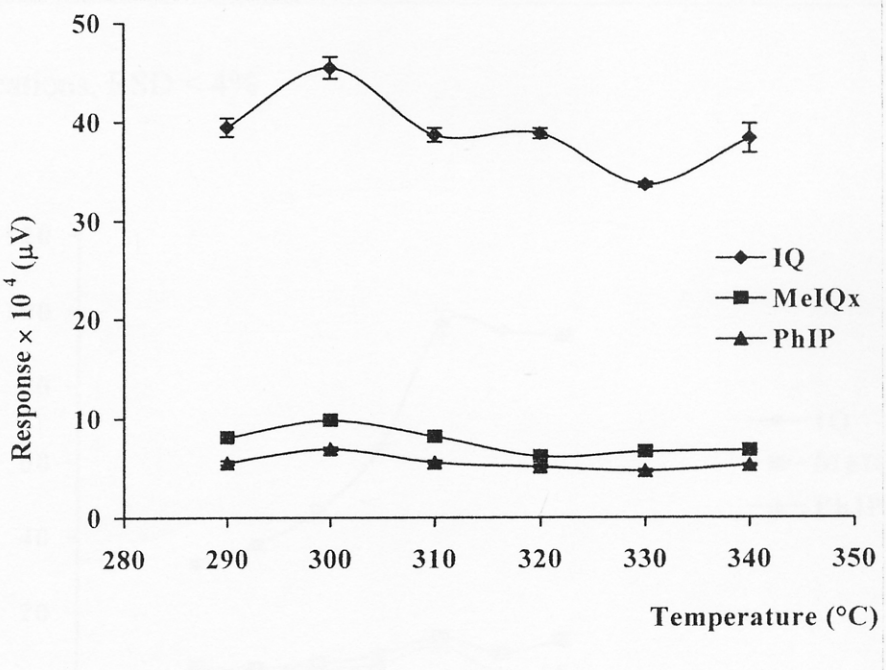

Figure 29 The responses of HCA derivatives at various injector temperatures

3.2.4 The detector temperature

The responses from various detector temperatures are shown in Table 22 and Figure 30. The highest response for all three HCA derivatives was obtained at 340°C and this was selected to be the optimum detector temperature.

Table 22 The responses of HCA derivatives at various detector temperatures

Detector temperature (°C)	Response* × 10^4 (μV) ± SD		
	IQ	MeIQx	PhIP
300	33.1 ± 1.1	5.5 ± 0.1	3.9 ± 0.1
310	38.3 ± 1.5	5.3 ± 0.2	4.2 ± 0.2
320	47.4 ± 1.1	6.9 ± 0.2	5.1 ± 0.2
330	64.1 ± 0.6	9.0 ± 0.2	6.7 ± 0.3
340	97.0 ± 3.4	14.0 ± 0.6	11.6 ± 0.2
350	95.0 ± 0.1	9.8 ± 0.2	4.2 ± 0.1
360	94.0 ± 1.6	13.5 ± 0.2	5.2 ± 0.1

* 5 replications, RSD < 4%

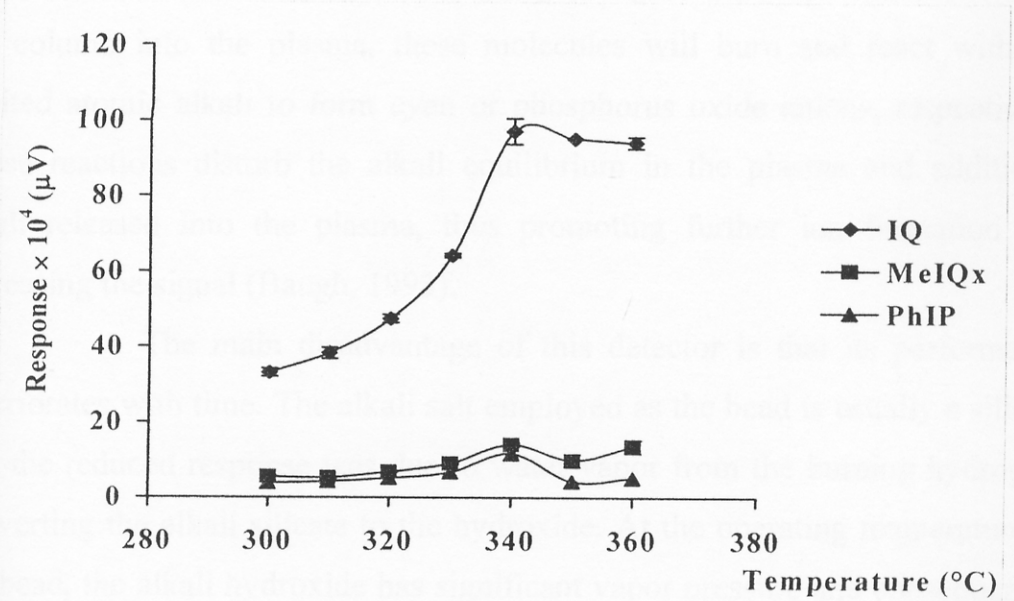

Figure 30 The responses of HCA derivatives at various detector temperatures

3.2.5 The fuel gas flow rate (Hydrogen gas)

Nitrogen phosphorus detector (also known as the thermic emission detector) is similar in design to the flame ionization detector (FID) but with an important difference, there is an electrically heated silicate bead doped with an alkali salt mounted between the jet and the collector (Figure 31). A very low hydrogen flow rate is mixed with the carrier gas and burns as plasma flame as it makes contact with the heated bead. The collector is maintained at a positive electrical polarity with respect to the bead and jet. The exact mechanism for producing a response has been subject of some discussion but Kolb's theory seems to be widely accepted (Tipler, 1993): at the operating temperature, the bead substrate is electrically conductive and some of the alkali ions are able to acquire an electron and are thus converted to the atomic form. These atoms are relatively volatile and are emitted into the plasma, where they quickly react with combustion products, and are ionized again and recollected on the negatively polarized bead. This repeated process gives rise to the background signal and explains why the bead continues to function over an extended time. If a compound containing nitrogen or phosphorus elutes from the column into the plasma, these molecules will burn and react with the excited atomic alkali to form cyan or phosphorus oxide anions, respectively. These reactions disturb the alkali equilibrium in the plasma and additional alkali released into the plasma, thus promoting further ion formation and increasing the signal (Baugh, 1993).

The main disadvantage of this detector is that its performance deteriorates with time. The alkali salt employed as the bead is usually a silicate that the reduced response was due to water vapor from the burning hydrogen, converting the alkali silicate to the hydroxide. At the operating temperature of the bead, the alkali hydroxide has significant vapor pressure and consequently, the rubidium or cesium is continually lost during the operating of the detector. Eventually all the alkali is evaporated, leaving a bead of inactive silica. This is

an inherent problem with all NPD detectors and as a result, the bead needs to replace regularly if the detector is in continuous use (Raymond, 1998).

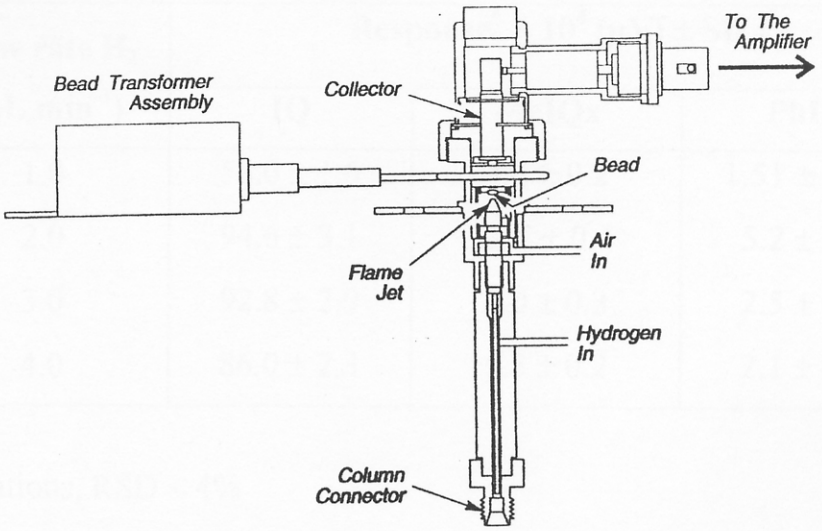

Figure 31 Nitrogen Phosphorus Detector (NPD)

In this system the analyte eluted from the column was detected by a nitrogen phosphorus detector (NPD). This detector consists of small hydrogen and air diffusion flame burning produced from oxidant and fuel gas. The oxidant gas was air and the fuel gas was hydrogen. Thus, the flow rate of air and hydrogen gases significant influence the noise level and the sensitivity of the detector.

The effect of hydrogen flow rate to the response is shown in Table 23 and Figure 32. The highest response was obtained at 2 mL min^{-1}, and this was selected as the optimum flow rate. This is the same as the recommended value of GC-NPD manual (2 mL min^{-1}).

Table 23 The effect of hydrogen gas flow rate on the responses of HCA derivatives

Flow rate H_2 (mL min^{-1})	Response* × 10^4 (μV) ± SD		
	IQ	MeIQx	PhIP
1.0	58.0 ± 1.6	4.2 ± 0.2	1.51 ± 0.05
2.0	94.6 ± 3.1	12.5 ± 0.4	5.2 ± 0.1
3.0	92.8 ± 2.9	7.0 ± 0.3	2.5 ± 0.1
4.0	86.0 ± 2.3	5.5 ± 0.2	2.1 ± 0.1

* 5 replications, RSD < 4%

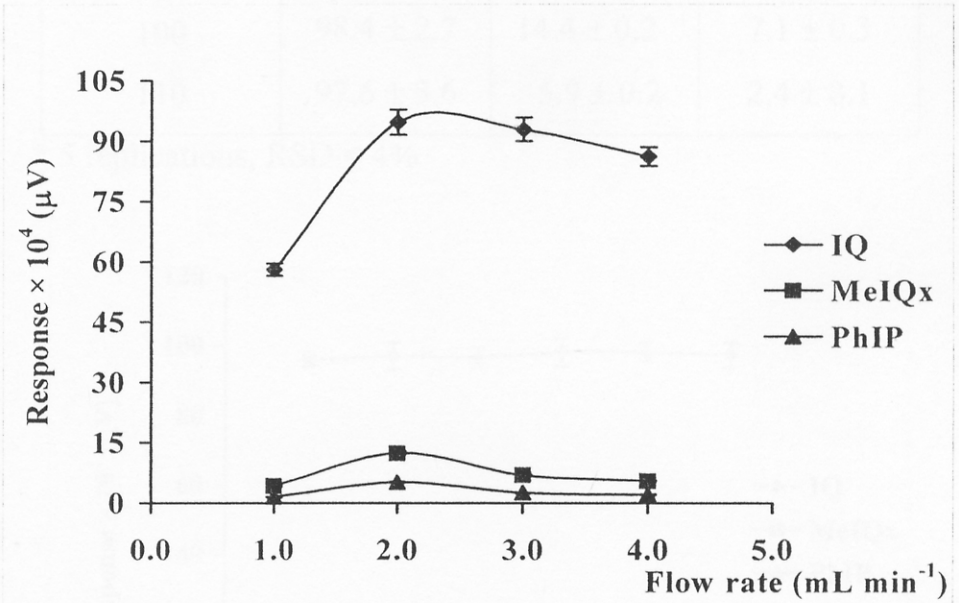

Figure 32 The effect of hydrogen gas flow rate on the responses of HCA derivatives

3.2.6 The oxidant flow rate (air)

Table 24 and Figure 33 show the responses obtained from experiment 2.4.6.6 The flow rate of 100 mL min^{-1} gave the highest response and was chosen as the optimum flow rate of air. From this study the optimum flow rate was also similar as the recommended value of GC-NPD manual (100 mL min^{-1}).

Table 24 The effect of air flow rate on the responses of HCA derivatives

Flow rate of Air (mL min^{-1})	Response* × 10^4 (μV) ± SD		
	IQ	MeIQx	PhIP
60	95.9 ± 1.7	6.4 ± 0.2	2.6 ± 0.1
70	97.1 ± 3.9	6.7 ± 0.2	3.1 ± 0.1
80	96.8 ± 3.0	13.2 ± 0.5	6.2 ± 0.2
90	98.4 ± 4.0	12.7 ± 0.4	5.6 ± 0.2
100	98.4 ± 2.7	14.4 ± 0.2	7.1 ± 0.3
110	97.6 ± 3.6	5.9 ± 0.2	2.4 ± 0.1

* 5 replications, RSD < 4%

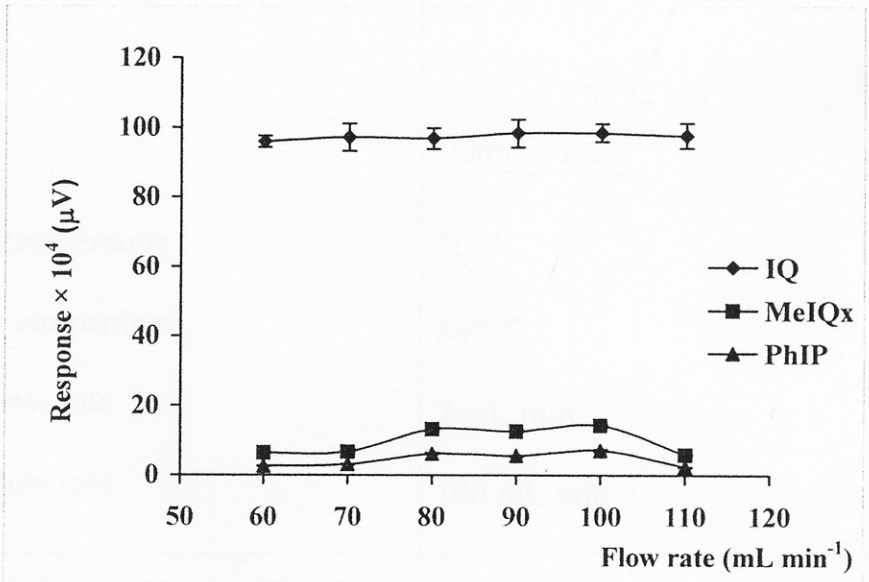

Figure 33 The effect of air flow rate on the responses of HCA derivatives

The optimum conditions for heterocyclic amines (IQ, MeIQx and PhIP) analysis on capillary column (PE-17 ht), 30 m x 0.25 mm I.D., × 0.25 μm with nitrogen phosphorus detector were summarized in Table 25. The chromatograms obtained from these optimum conditions gave a high resolution (R>>1) (Figure 34).

Table 25 The optimum conditions of GC-NPD

Parameters	Optimum values
GC-NPD	
Column	PE-17, 30 m × 0.25 mm I.D., 0.25 μm film thickness of 50% phenyl-50% methylpolysiloxane
Carrier gas flow rate	1.5 mL min^{-1}
Column temperature programmed	330°C, 5 min 10°C/ min 280°C, 0 min 35°C/ min 190°C, 3 min
Injector temperature	300°C
Detector temperature	340°C
H_2 gas flow rate	2 mL min^{-1}
O_2 gas flow rate	100 mL min^{-1}

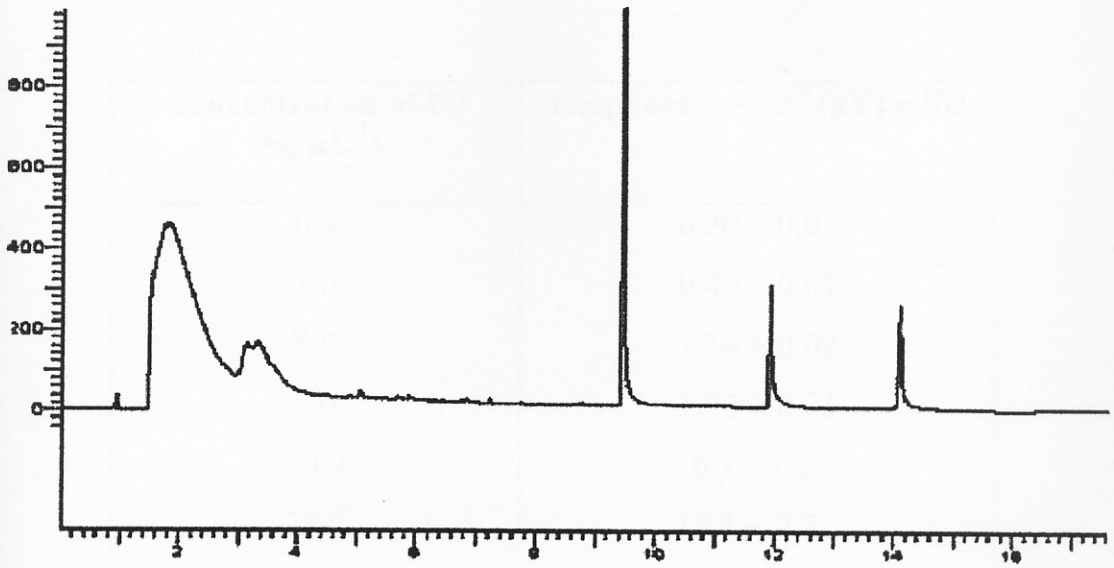

Figure 34 The chromatograms of three HCAs derivatives at optimum conditions on capillary column (PE-17 ht) with GC-NPD

3.2.7 Linear dynamic range (LDR)

The linear dynamic range, LDR is the characteristic of the detector. It is the concentration where the range detector response is linear. In experiment 2.4.7 the linear dynamic range was investigated by varied the concentration then plotted against the response. Table 26-28 and Figure 35-37 shown the response and linear regression, R^2, of individual HCAs at various concentrations. From the results provided a wide linear dynamic range from 0.8 to 100.0 ng μL^{-1} with good linear regression $R^2 > 0.99$.

Table 26 The responses of IQ derivative at various concentrations

Concentration of IQ (ng μL^{-1})	Response * $\times 10^{4}$ (μV) ± SD
0.8	0.20 ± 0.01
1.0	0.40 ± 0.01
3.0	1.10 ± 0.02
5.0	1.70 ± 0.03
10.0	6.7 ± 0.2
25.0	15.3 ± 0.2
50.0	36.4 ± 0.5
80.0	51.2 ± 1.8
100.0	62.1 ± 1.2

*5 replications, RSD < 4%

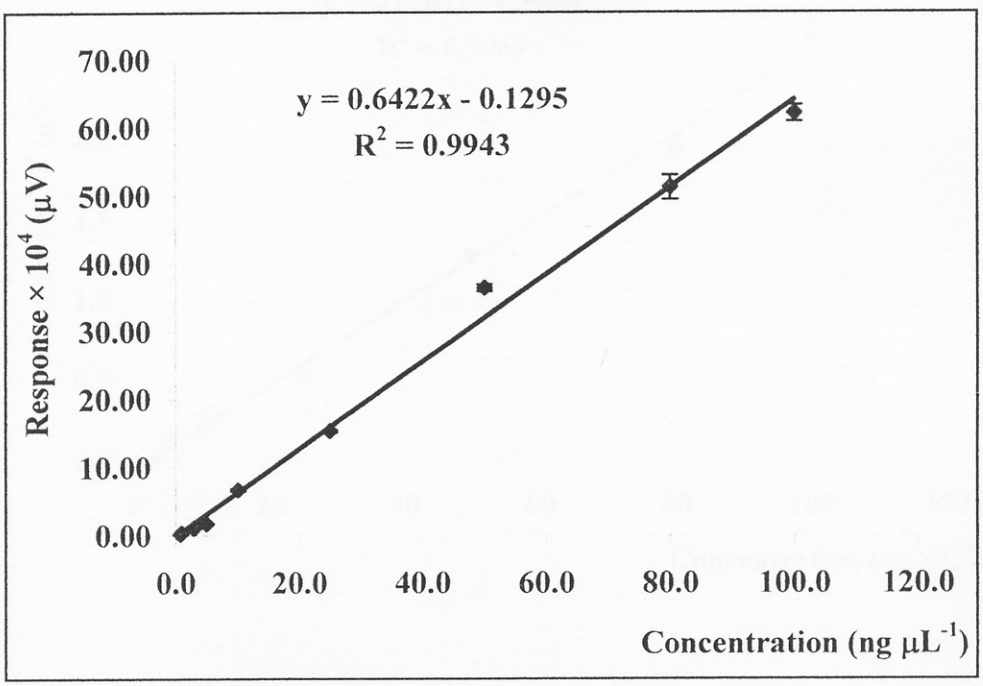

Figure 35 The linear dynamic range of IQ derivative

Table 27 The responses of MeIQx derivative at various concentrations

Concentration (MeIQx) ($ng\ \mu L^{-1}$)	Response* $\times 10^4$ (μV) $\pm$ SD
3.0	0.020 ± 0.003
5.0	0.130 ± 0.004
10.0	0.20 ± 0.01
25.0	0.50 ± 0.01
50.0	1.30 ± 0.03
80.0	2.0 ± 0.1
100.0	2.6 ± 0.1

*5 replications, RSD < 4%

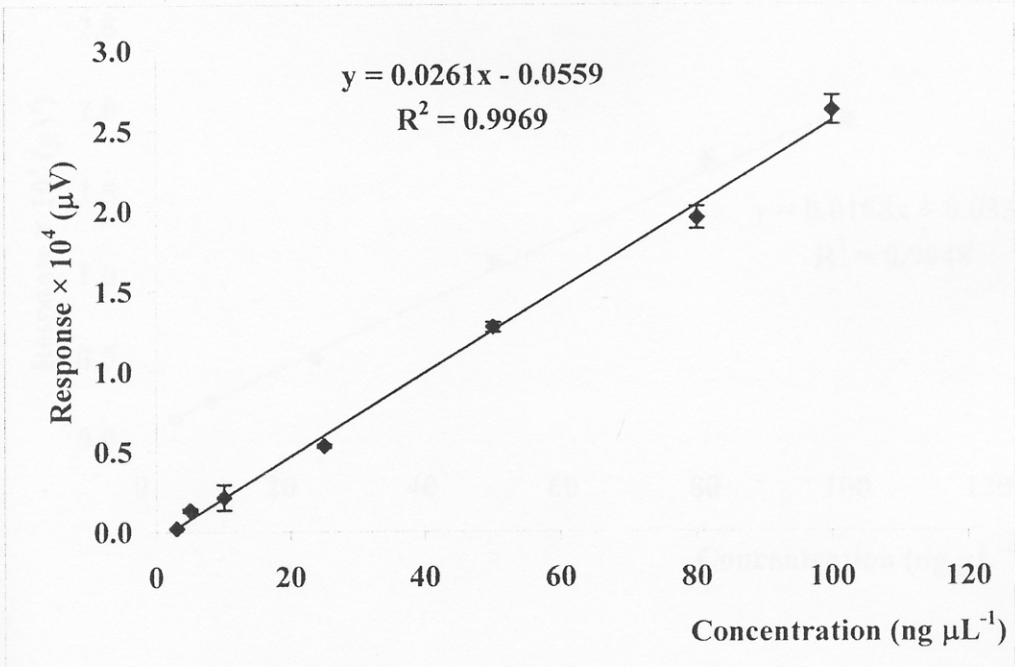

Figure 36 The linear dynamic range of MeIQx derivative

Table 28 The responses of PhIP derivative at various concentrations

Concentration (PhIP) (ng μL^{-1})	Response* $\times 10^4$ (μV) $\pm$ SD
5.0	0.120 $\pm$ 0.002
10.0	0.23 $\pm$ 0.01
25.0	0.50 $\pm$ 0.01
50.0	1.10 $\pm$ 0.04
80.0	1.7 $\pm$ 0.1
100.0	1.9 $\pm$ 0.1

*5 replications, RSD < 4%

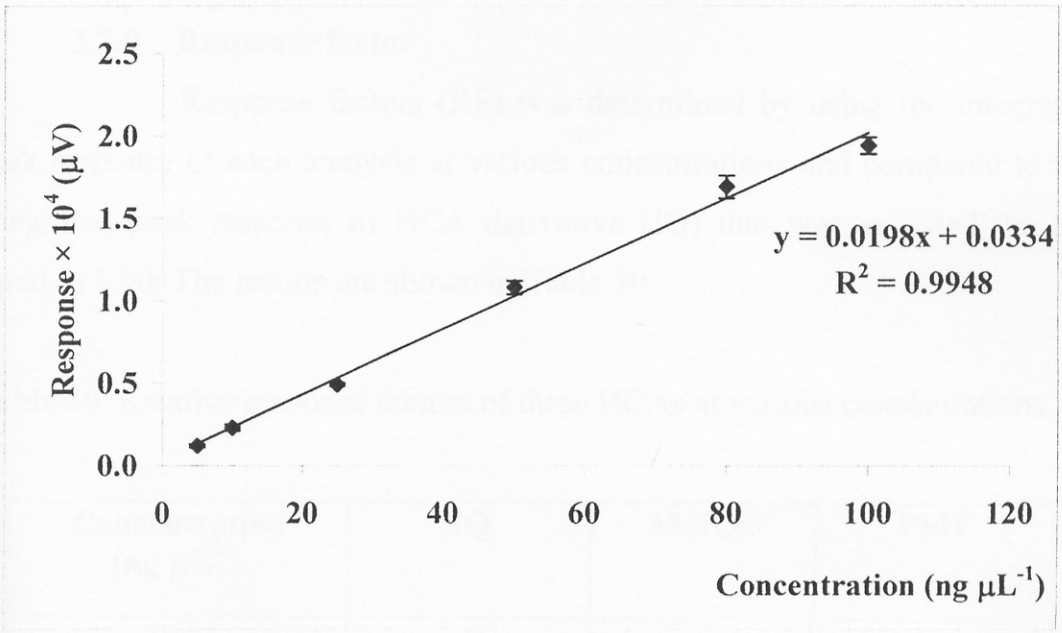

Figure 37 The linear dynamic range of PhIP derivative

3.2.8 Limit of detection

The limit of detection was defined as the concentration of HCAs where S/N is more than 3.0. These are shown in the Table 29. The different response of the NPD to each HCA was due to the structure of the compound (see Figure 10-12).

Table 29 The limit of detection of three HCAs with S/N ≥ 3.

HCAs	Concentration (ng μL^{-1})
IQ	0.5
MeIQx	3.0
PhIP	5.0

*5 replications, RSD < 4%

3.2.9 Response factor

Response factors (RF) was determined by using the integrated peak response of each analysis at various concentrations and compared to the integrated peak response of HCA derivative (IQ) that was assigned the RF equal to 1.00. The results are shown in Table 30

Table 30 Relative response factors of three HCAs at various concentrations

Concentration (ng μL^{-1})	IQ	MeIQx	PhIP
1.0	1.00	-	-
5.0	1.00	0.76	0.71
10.0	1.00	0.31	0.29
25.0	1.00	0.35	0.33
50.0	1.00	0.35	0.30

*5 replications, RSD < 4%

3.3 Confirmation of the HCA derivative structures

The structures of the HCA derivatives were confirmed by GC-MS analysis. The aminoazzaarenes were analyzed as N-dimethylaminomethylene methyl ester derivatives. Figures 38- 41 presented the total ion chromatogram and characteristic mass chromatogram of N-dimethylaminomethylene derivatives of IQ, MeIQx and PhIP. A molecular ion peak [M^+] was observed for each of the derivatives and other common ion peaks which were useful for structure elucidation were [M-15]$^+$ (CH_3), [M-44]$^+$[$N(CH_3)_2$], [M-56]$^+$[$C{=}N(CH_3)_2$] and [M-71]$^+$[$N{=}CHN(CH_3)_2$].

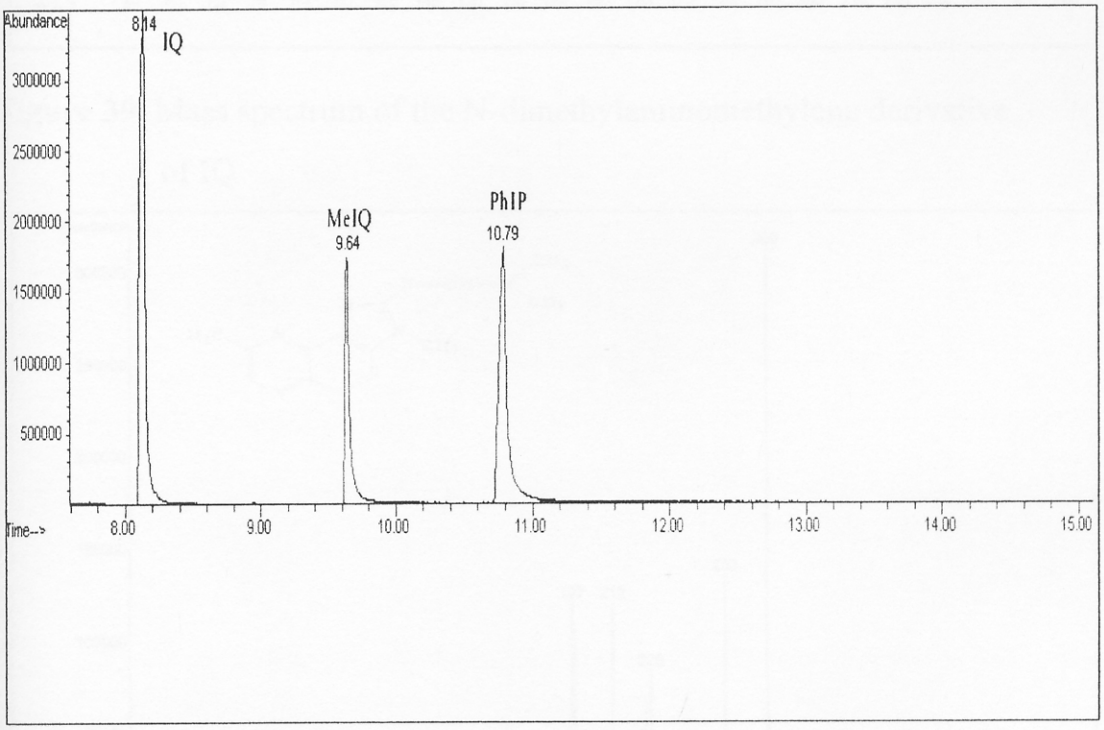

Figure 38 Total ion chromatograms of heterocyclic amine derivatives confirmed by GC-MS

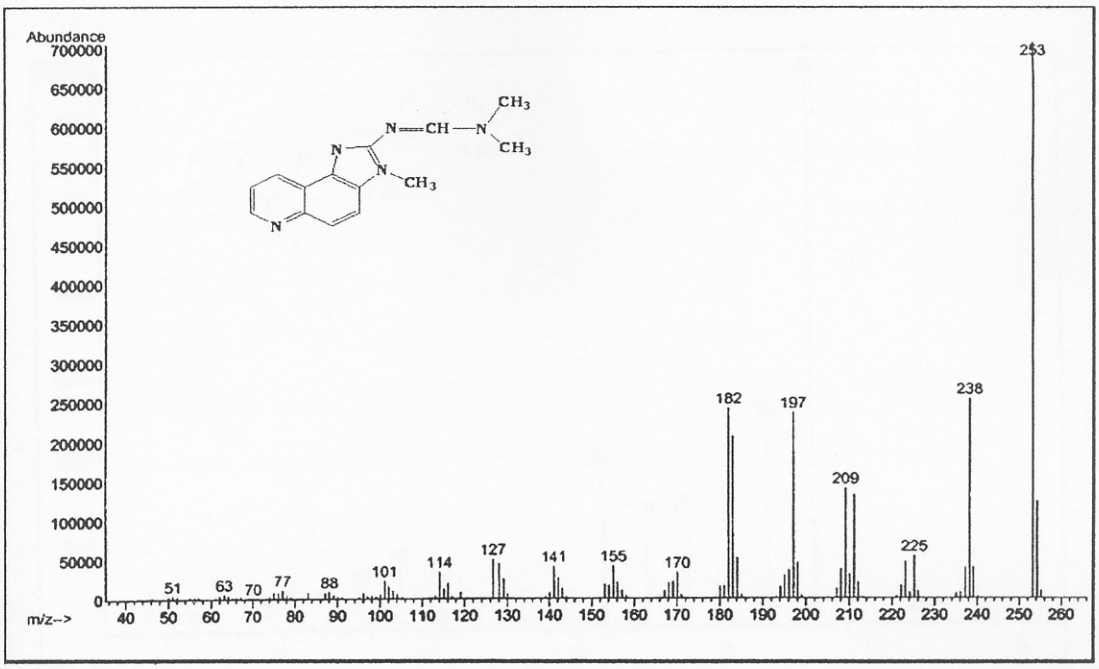

Figure 39 Mass spectrum of the N-dimethylaminomethylene derivative of IQ

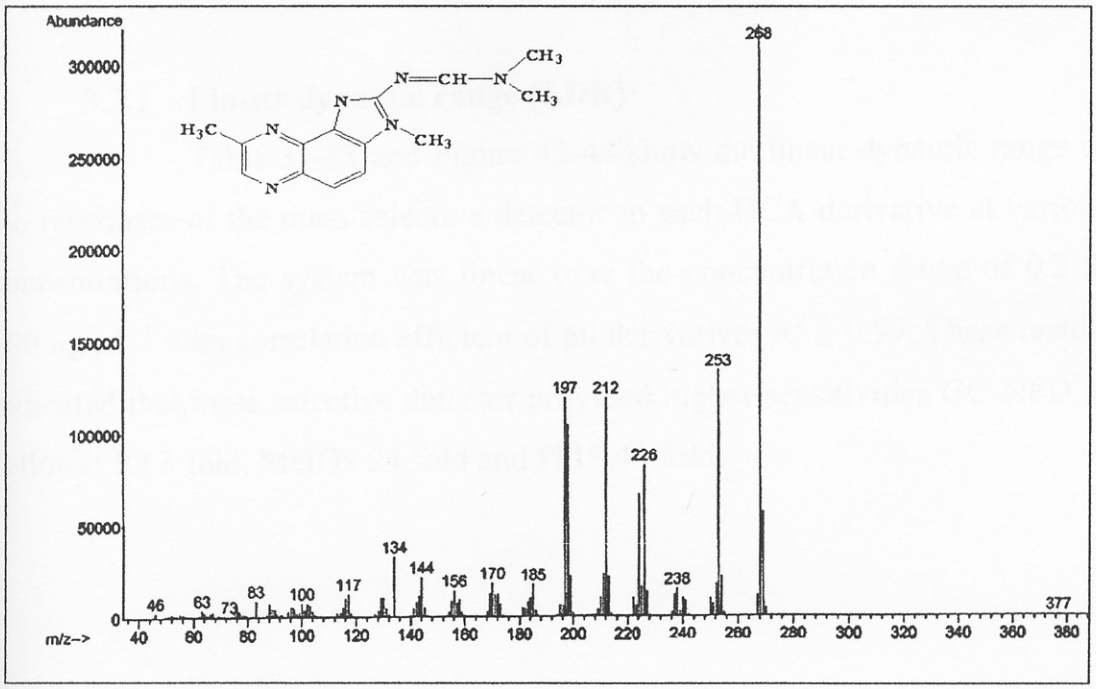

Figure 40 Mass spectrum of the N-dimethylaminomethylene derivative of MeIQx

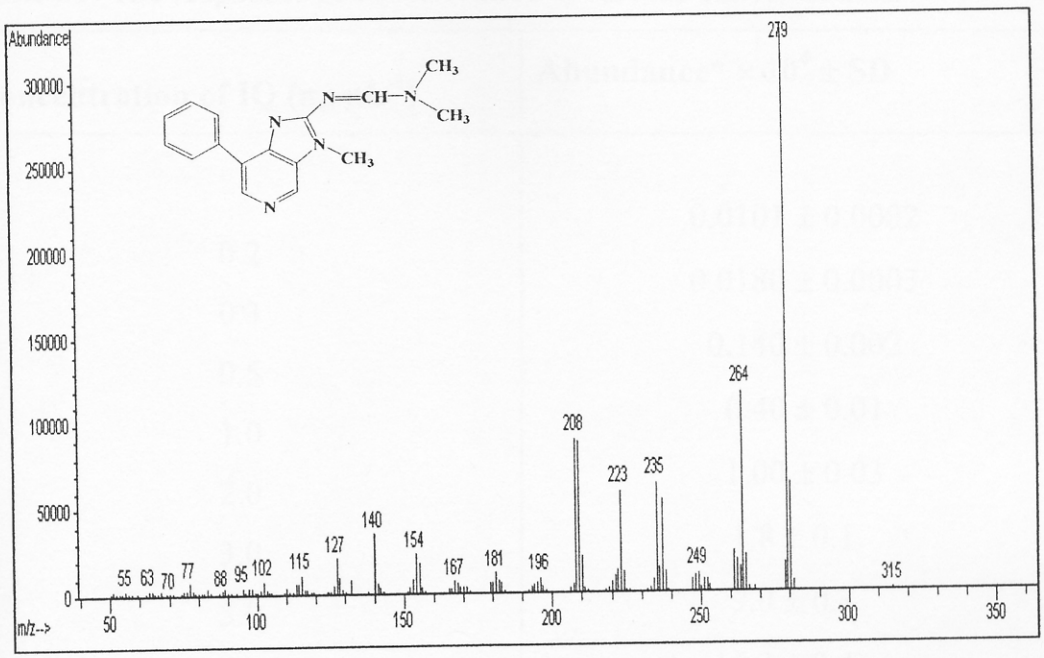

Figure 41 Mass spectrum of the N-dimethylaminomethylene derivative of PhIP

3.3.1 Linear dynamic range (LDR)

Table 31-33 and Figure 42-44 show the linear dynamic range of the responses of the mass selective detector to each HCA derivative at various concentrations. The system was linear over the concentration range of 0.2 to 100 ng μL^{-1} with correlation efficient of all derivatives $R^2 \geq 0.99$. These results indicated that mass selective detector provided higher sensitivities GC-NPD as follows: IQ 3 fold, MeIQx 24 fold and PhIP 44 fold.

Table 31 The responses of IQ derivative at various concentrations

Concentration of IQ (ng μL^{-1})	Abundance* $\times 10^4 \pm$ SD
0.2	0.0101 ± 0.0002
0.3	0.0180 ± 0.0003
0.5	0.140 ± 0.002
1.0	0.40 ± 0.01
2.0	1.00 ± 0.03
3.0	1.8 ± 0.1
5.0	9.0 ± 0.3
10.0	15.3 ± 0.4
50.0	92.0 ± 1.9
100.0	206.3 ± 8.0

* 5 replications, RSD < 4%

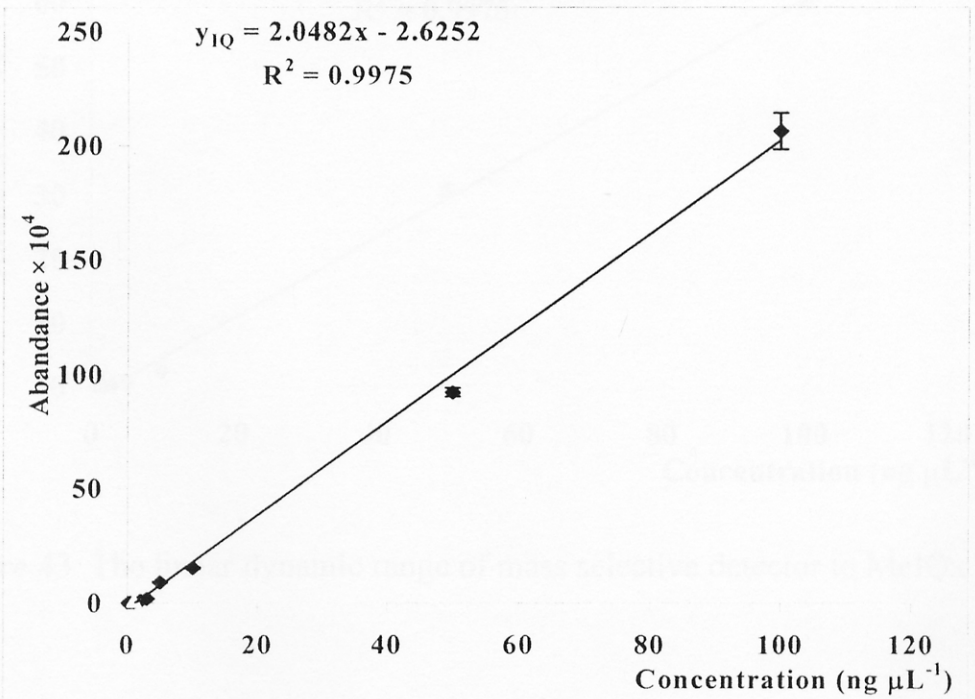

Figure 42 The linear dynamic range of mass selective detector to IQ

Table 32 The responses of MeIQx derivative at various concentrations

Concentration of MeIQx ($ng\ \mu L^{-1}$)	Abundance* $\times 10^4 \pm$ SD
1.0	0.0120 ± 0.0002
2.0	0.0230 ± 0.0004
3.0	0.06 ± 0.002
5.0	0.60 ± 0.01
10.0	2.4 ± 0.1
50.0	30.7 ± 1.0
100.0	60.1 ± 1.0

* 5 replications, RSD < 4%

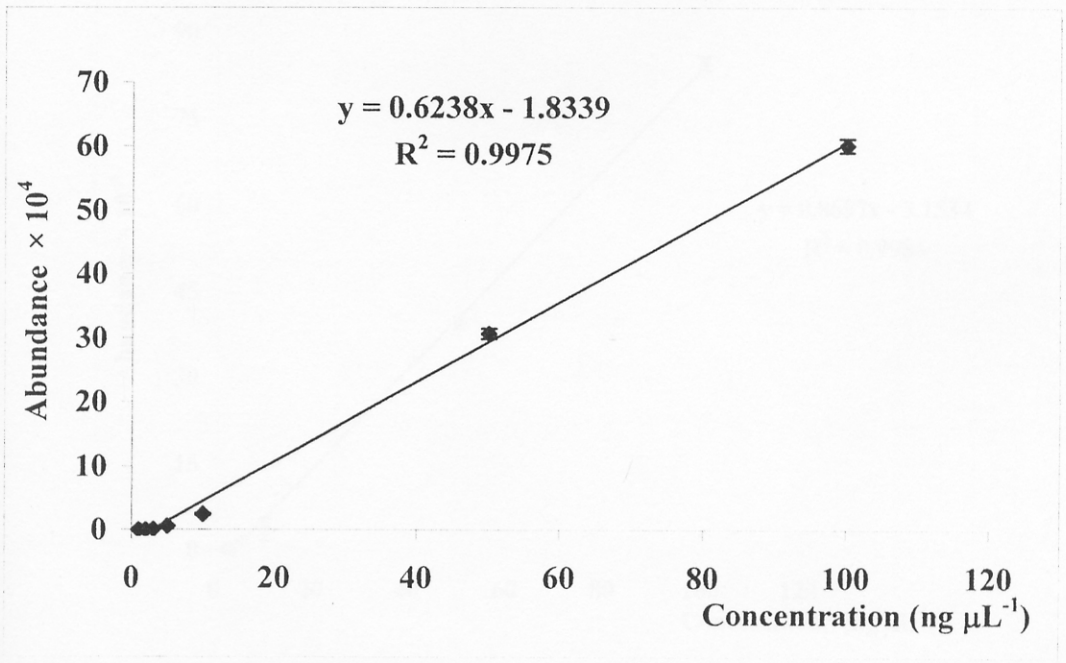

Figure 43 The linear dynamic range of mass selective detector to MeIQx

Table 33 The responses of PhIP derivative at various concentrations

Concentration of PhIP (ng μL^{-1})	Abundance* $\times 10^4$ $\pm$ SD
2.0	0.0140 $\pm$ 0.0003
3.0	0.04 $\pm$ 0.001
5.0	1.60 $\pm$ 0.01
10.0	3.5 $\pm$ 0.1
50.0	39.3 $\pm$ 1.1
100.0	84.4 $\pm$ 1.2

* 5 replications, RSD < 4%

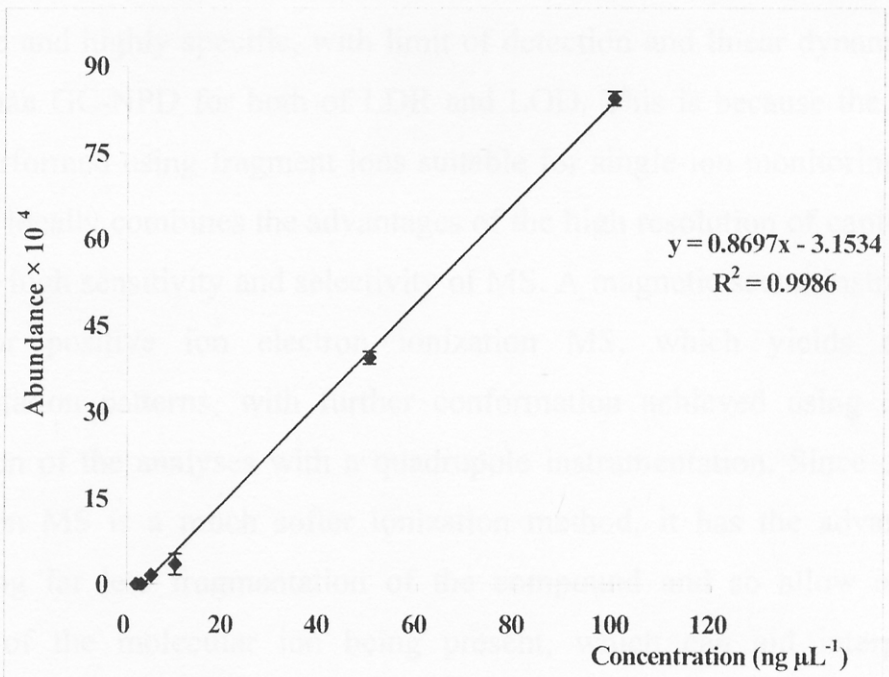

Figure 44 The linear dynamic range of mass selective detector to PhIP

3.3.2 Limit of detection (LOD)

The limit of detection of each HCA derivative was shown in the Table 34. These the results indicated that mass selective detector gave a high sensitivity and better than those obtained from GC-NPD.

Table 34 The limit of detection of three HCAs with S/N ≥ 3.

HCAs	Limit of detection ($ng\ \mu L^{-1}$)
IQ	0.1
MeIQx	1.0
PhIP	1.0

* 5 replications, RSD < 4%

From the results, GC-MS method was shown to be very sensitive and highly specific, with limit of detection and linear dynamic range better than GC-NPD for both of LDR and LOD. This is because the analytes were performed using fragment ions suitable for single-ion monitoring (SIM). GC-MS ideally combines the advantages of the high resolution of capillary GC with the high sensitivity and selectivity of MS. A magnetic sector instrument is used for positive ion electron ionization MS, which yields excellent fragmentation patterns, with further conformation achieved using chemical ionization of the analyses with a quadrupole instrumentation. Since chemical ionization MS is a much softer ionization method, it has the advantage of producing far less fragmentation of the compound and so allow a greater chance of the molecular ion being present, which can aid interpretation (Kataoka, 1997). GC-MS offers high specificity and selectivity for the determination HCAs. However, authors reported interference complex in food samples cause contamination of ion source through the deposition of non- volatile material, and column lifetime is short (Pais and Knize ,2000).

3.4 Comparison of two different capillary columns

The comparison of the two columns, PE-17ht (Table 24) and HP-5was done by setting the GC conditions at the optima summarized in Table 35. The chromatograms obtained from these optimum conditions gave high resolution (R>>1) (Figure 45).

Table 35 The optimum conditions of GC-NPD equipped with HP-5 column

Parameters	Optimum values
GC-NPD	
Column	HP-5, 30 m × 0.32 mm I.D., 0.25 μm film thickness of 5% phenyl-95%methylpolysiloxane
Carrier gas flow rate	1.5 mL min^{-1}
Column temperature programmed	300°C, 5 min / 280°C, 0 min / 35°C/ min / 190°C, 3 min
Injector temperature	300°C
Detector temperature	300°C
H_2 gas flow rate	2 mL min^{-1}
O_2 gas flow rate	100 mL min^{-1}

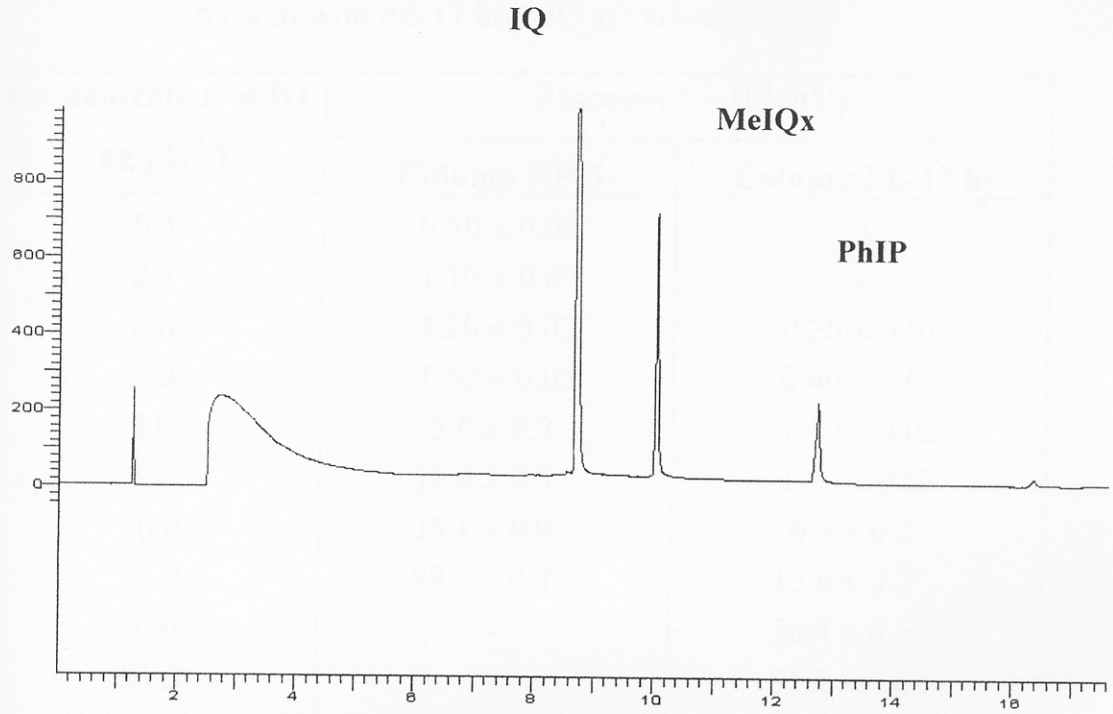

Figure 45 The chromatograms of three HCAs at optimum conditions on HP-5 capillary column

3.4.1 Linear dynamic range of HP-5 compared with PE-17 ht

Tables 36-38 and Figures 45-47 shown the linear dynamic range of the response of the nitrogen phosphorus selective detector to each HCA derivative at various concentrations. The system is linear over the concentration range with correlation efficient of all derivatives $R^2 \geq 0.99$. HP-5 capillary column equipped with GC-NPD gave a higher sensitivity than those obtained from PE-17 ht capillary column *i.e.* IQ 6 fold, MeIQx 65 fold and PhIP 19 fold

Table 36 The linear dynamic range of the response of HP-5 compared with PE-17 ht to IQ at various

Concentration of IQ ($ng\ \mu L^{-1}$)	Response* $\times 10^4$ (μV)	
	Column HP-5	Column PE-17 ht
0.3	0.50 ± 0.02	-
0.5	1.10 ± 0.03	-
0.8	1.20 ± 0.02	0.20 ± 0.01
1.0	1.60 ± 0.05	0.40 ± 0.01
3.0	5.0 ± 0.2	1.10 ± 0.02
5.0	11.6 ± 0.3	1.70 ± 0.03
10.0	35.1 ± 0.9	6.7 ± 0.2
25.0	98.3 ± 0.3	15.4 ± 0.2
50.0	-	36.4 ± 0.5
80.0	-	51.2 ± 1.8
100.0	-	62.1 ± 1.2

* 5 replications, RSD < 4%

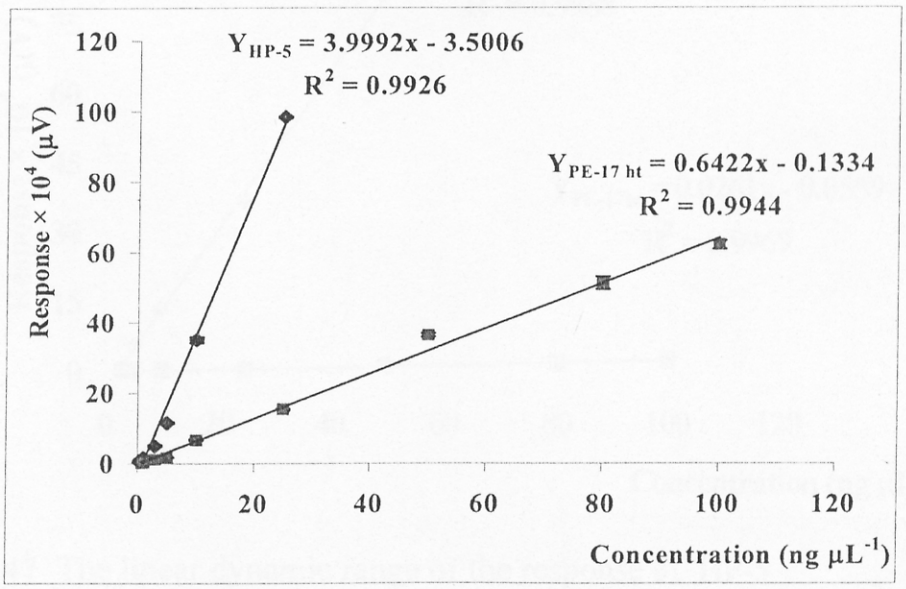

Figure 46 The linear dynamic range of the response of HP-5 compared with PE-17 ht to IQ at various concentrations

Table 37 The linear dynamic range of the response of HP-5 compared with PE-17 ht to MeIQx at various

Concentration of MeIQx (ng μL^{1})	Response*$\times 10^{4}$ (μV)	
	Column HP-5	Column PE-17 ht
3	0.50 ± 0.02	0.020 ± 0.003
5	5.6 ± 0.2	0.130 ± 0.004
10	13.5 ± 0.7	0.20 ± 0.01
25	36.8 ± 0.8	0.50 ± 0.01
50	81.8 ± 0.4	1.30 ± 0.03
80	-	2.0 ± 0.1
100		2.6 ± 0.1

* 5 replications, RSD < 4%

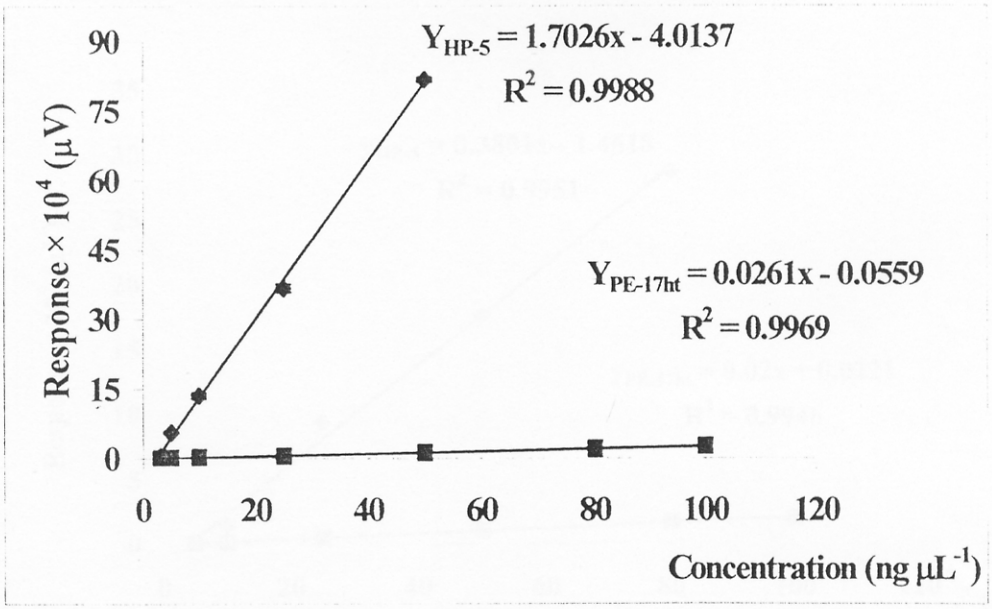

Figure 47 The linear dynamic range of the response of HP-5 compared with PE-17 ht to MeIQx at various concentrations

Table 38 The linear dynamic range of the response of HP-5 compared with PE-17 ht to PhIP at various concentrations

Concentration of PhIP ($ng\ \mu L^{-1}$)	Response* $\times 10^4$ (μV) $\pm$ SD	
	Column HP-5	Column PE-17 ht
5	0.20 ± 0.01	0.120 ± 0.002
10	1.50 ± 0.02	0.23 ± 0.01
25	9.4 ± 0.2	0.50 ± 0.01
50	17.6 ± 0.2	1.10 ± 0.04
80	28.7 ± 0.4	1.7 ± 0.1
100	-	1.9 ± 0.1

5 replications, RSD < 4%

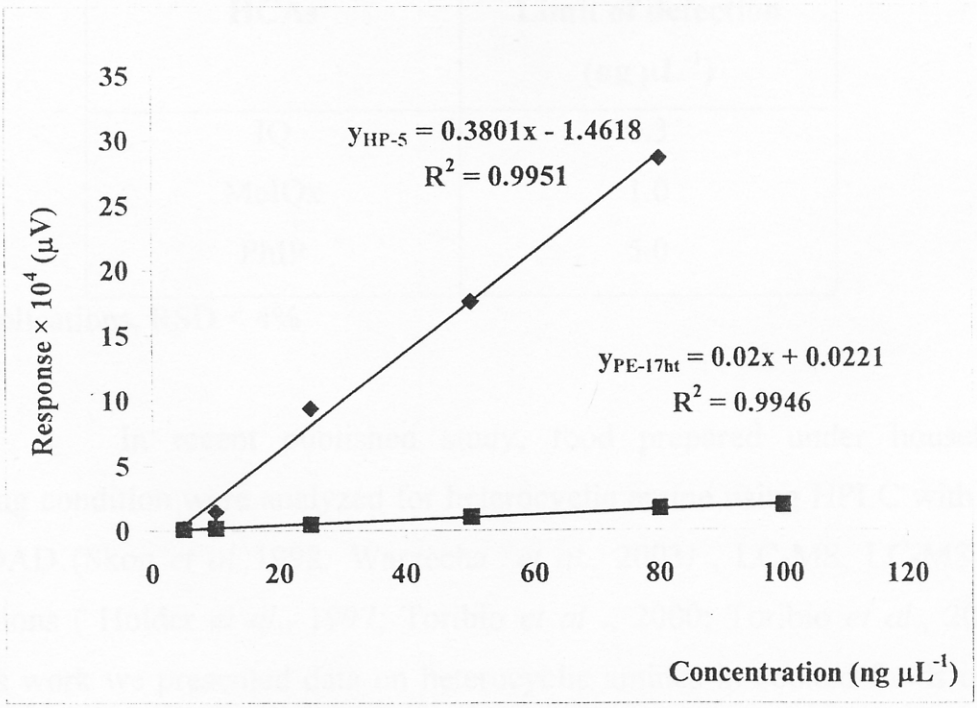

Figure 48 The linear dynamic range of the response of HP-5 compared with PE-17 ht to PhIP at various concentrations

3.4.2 Limit of detection (LOD)

The limit of detection of each HCA derivatives is shown in Table 39. These results indicated that when the analysis using HP-5 capillary column equipped with GC-NPD gave a higher sensitivity than those obtained from PE-17 ht capillary column. Usually, heterocyclic amines were analyzed by GC technique using various capillary columns, such as Rtx-50 (50%phenyl–50% methylpolysiloxane) 30m x 0.32 mm I.D., 0.50 μm film thickness (Skog *et al.*, 1998) DB-17ht (50%phenyl-50%methylpolysiloxane) (10m x 0.25 mm x 0.15 μm film thickness high temperature (Kataoka and Koji, 1997). It is shown here that an HP-5 capillary column, a common column use in general laboratory, can also be used. However, for PE-17 ht due to the high temperature for heterocyclic amines (IQ, MeIQx and PhIP) analysis column lifetime is rather short.

Table 39 The limit of detection of three HCAs with S/N ≥ 3

HCAs	Limit of detection ($ng\ \mu L^{-1}$)
IQ	0.3
MeIQx	1.0
PhIP	5.0

* 5 replications, RSD < 4%

In recent published study, food prepared under household cooking condition were analyzed for heterocyclic amine using HPLC with UV and DAD (Skog *et al.*, 1998; Warzecha *et al.*, 2003) , LC-MS, LC-MS-MS detections (Holder *et al.*, 1997; Toribio *et al* ., 2000; Toribio *et al.*, 2002). In this work we presented data on heterocyclic amines in cooked foods using a gas chromatography-nitrogen phosphorus detector coupling with capillary column, HP-5 with derivatization of the compounds

3.5 Sample preparation optimization

3.5.1 The extraction time

The extraction time was the time necessary to achieve a complete release of heterocyclic amines from matrix by ultrasonic extraction in the initial alkaline treatment. To check the influence of the extraction time in the initial alkaline treatment, once the sample was homogenized in the sodium hydroxide solution, the extraction time was varied from 30 minutes to 3 hours with an increment of 30 minutes. The results are in Table 40 and Figure 49. IQ gave the highest response at 1 hour, but MeIQx and PhIP both gave low response. Since the analysis of HCAs would be performed simultaneously 2 hours was selected as the optimum extraction time since it gave high response for all HCA. This extraction time was shorter than obtained by Toribio *et al.* (2000) which the analysis was done by sonication for 3 hours.

3.5.2 The flow rate of eluting solvent

Table 41 and Figure 50 show the responses at different flow rates. A flow rate of 2 mL min^{-1} that provided the highest response. Therefore, 2 mL min^{-1} was selected as the optimum flow rate.

Table 40 The responses of three HCAs at various extraction times

Extraction time (minutes)	Response*× 10^4 (μV) ± SD		
	IQ	MeIQ	PhIP
30	11.1 ± 1.1	9.7 ± 0.2	4.5 ± 0.5
60	82.7 ± 4.4	3.2 ± 0.3	1.2 ± 0.1
90	18.6 ± 2.0	1.1 ± 0.1	0.50 ± 0.02
120	47.4 ± 5.6	19.7 ± 1.0	10.1 ± 0.5
150	32.3 ± 1.6	0.8 ± 0.1	1.5 ± 0.1
180	6.2 ± 0.6	3.1 ± 0.3	1.9 ± 0.1

* 5 replications, RSD ≤ 10%

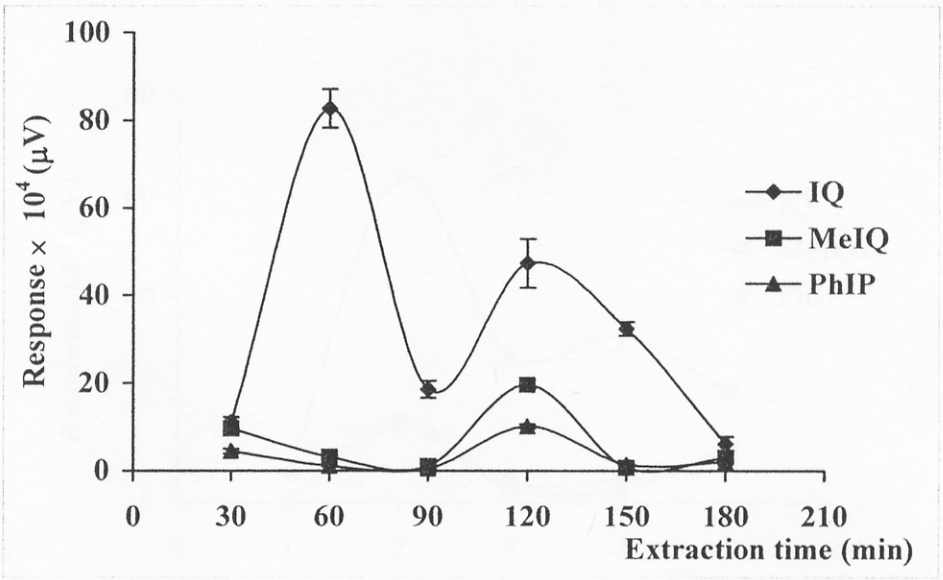

Figure 49 The responses of three HCAs at various extraction times

Table 41 The responses of HCAs at various flow rates

Flow rate (mL/min)	Response*× 10^4 (μV) ± SD		
	IQ	MeIQx	PhIP
1	5.4 ± 0.6	0.21± 0.02	0.12 ± 0.01
2	63.6 ± 1.1	16.2 ± 0.4	14.7 ± 1.2
3	29.0 ±1.8	4.0± 0.4	2.7 ± 0.2
4	32.6 ± 2.6	4.4 ± 0.4	2.5 ± 0.2
5	21.5 ± 1.2	6.5 ± 0.4	10.8 ± 0.9

* 5 replications, RSD ≤ 10%

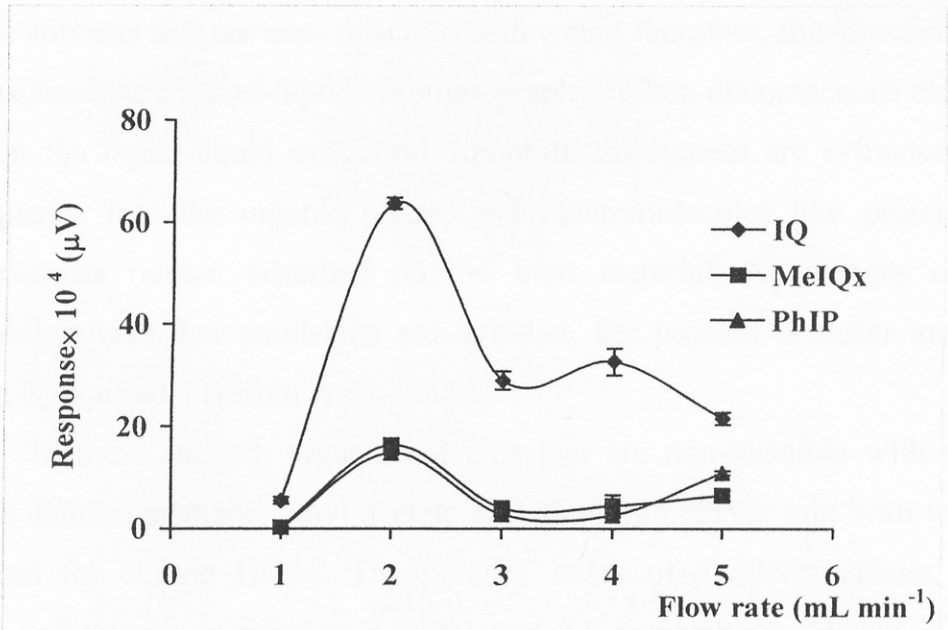

Figure 50 The responses of three HCAs at various flow rates

3.5.3 Selection of eluting solvent

Experiment 2.4.12.3 studied the suitable solvent for eluting HCAs that were adsorbed on the diatomaceous earth (mined from the fossilzed remains of diatoms, microscopic sea creatures). It is composed of silicon dioxide (SiO_2), a sand-like porous material. Diatomaceous earth is chemically inert substance that is used as a dehydrating agent because the small particles absorb moisture and oil (http://www.ipmofalaska.com/files/DE.html).

The use of diatomaceous earth as solid support for liquid-liquid extraction is recommended for sample preparation of aqueous samples. When this material is mixed with the sample, which has been previously homogenized in sodium hydroxide solution, the aqueous phase is distributed itself in the form of a thin film over the chemically inert matrix. Subsequently, HCAs are eluted using organic solvents that are non- miscible with water, therefore, this process could be considered as a liquid-liquid chromatography. When diatomaceous earth are used for the liquid-liquid extraction, lipophilic substances are extracted from the aqueous into the organic phase, and macromolecules like protein and carbohydrates remain adsorbed on the inert material. Advantages of this methodology are that emulsions are avoided, the process is faster and less solvent is required. (Toribio *et al.*, 2000).

In these studied, organic solvents that are non-miscible with water, such as dichloromethane, ethyl acetate and dichloromethane mix with toluene were test for eluting HCAs. The polarity index of dichloromethane, ethyl acetate and toluene is equal to 4.4, 3.1 and 2.4 respectively (Harvey, 2000). From the results (Table 42 and Figure 51) HCAs eluted with mixture solvent that contains toluene in dichloromethane gave better response than dichloromethane and ethyl acetate. It was also found that the system elute with ethyl acetate gave more interference, therefore, 5%toluene in dichloromethane was chosen to be an appropriate solvent for eluting HCAs from diatomaceous

earth .This results obtained were agreed with the work of Knize *et al.,* (1997), Pais *et al.,* (1999) and Janoszka *et al.*, (2001).

Table 42 The responses of three HCAs eluted from diatomaceous earth with 5%toluene in dichloromethane, dichloromethane, ethyl acetate

Type of eluting solvent	Response* × 10^4 (μV) ± SD		
	IQ	MeIQx	PhIP
5%Toluene+dichloromethane	55.6± 2.6	16.6 ± 1.8	16.6 ± 1.0
Dichloromethane	52.4 ± 2.3	16.2 ± 1.4	14.7 ± 1.2
Ethyl acetate	33.9 ± 2.8	15.5 ±1.3	14.9 ± 1.4

*5 replications, RSD ≤ 10 %

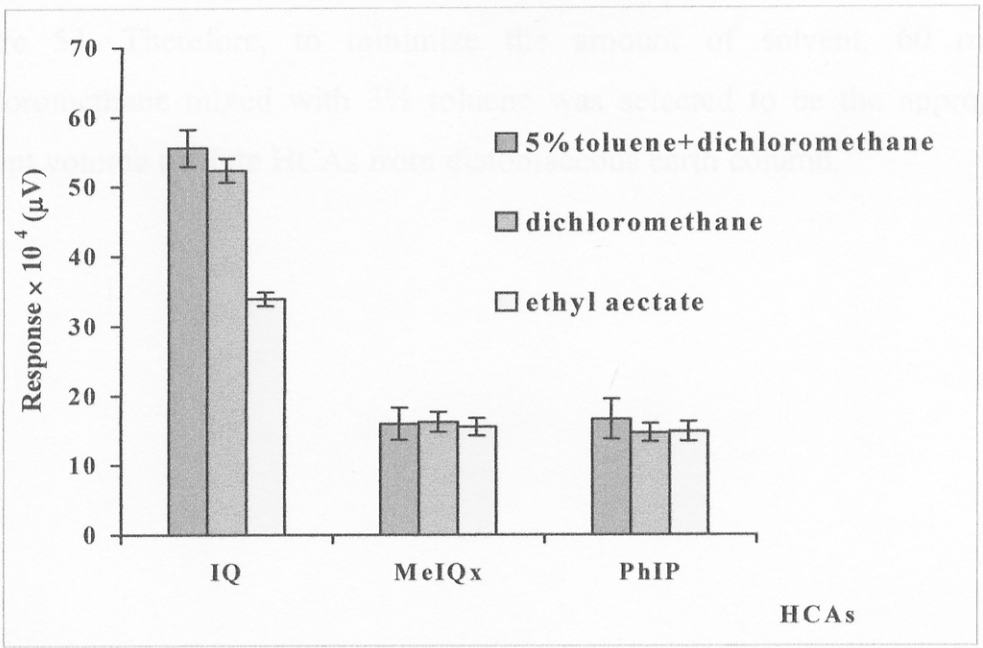

Figure 51 The responses of three HCAs eluted from diatomaceous earth with 5%toluene in dichloromethane, dichloromethane, ethyl acetate

3.5.4 Optimization of toluene amount

Table 43 and Figure 52 show the response of each HCA derivatives after investigated for the extraction efficiency with various percentage of toluene. A 3% (v/v) toluene mix with dichloromethane was the appropriate ratio to be used since it provided the high extraction efficiency and showed the best response. The amount of toluene in this work was less than the work of Janoszka and coworkers (2001) *i.e.* 5% toluene was used for analysis heterocyclic amines (aminoazaarenes) from meat samples.

3.5.5 Amount of eluting solvent

The volume of organic solvent used in extraction processes was important parameter because it would affect the extraction efficiency. If the volume is too small it may not be sufficient to elute the analyte on the diatomaceous earth. Therefore, it was necessary to optimize the volume of eluting solvent. Experiment 2.4.12.5 varied the volume of dichloromethane mixed with 3% toluene (eluent) and results obtained were in Table 44 and Figure 53. Therefore, to minimize the amount of solvent, 60 mL of dichloromethane mixed with 3% toluene was selected to be the appropriate solvent volume to elute HCAs from diatomaceous earth column.

Table 43 Responses using various amount of toluene in mixed solvents

Percentage of toluene (v/v)	Response* × 10^4 (μV) ± SD		
	IQ	MeIQx	PhIP
1	2.9 ± 0.1	0.40 ± 0.04	0.40 ± 0.03
2	7.9 ± 0.2	3.9 ± 0.2	3.5 ± 0.3
3	15.2 ± 1.2	13.3 ± 1.4	9.8 ± 1.0
4	9.5 ± 1.0	4.4 ± 0.3	3.5 ± 0.3
5	2.9 ± 0.2	0.3 ± 0.03	0.20 ± 0.02
7	0.9 ± 0.1	0.3 ± 0.02	0.1 ± 0.01

*5 replications, RSD ≤ 10 %

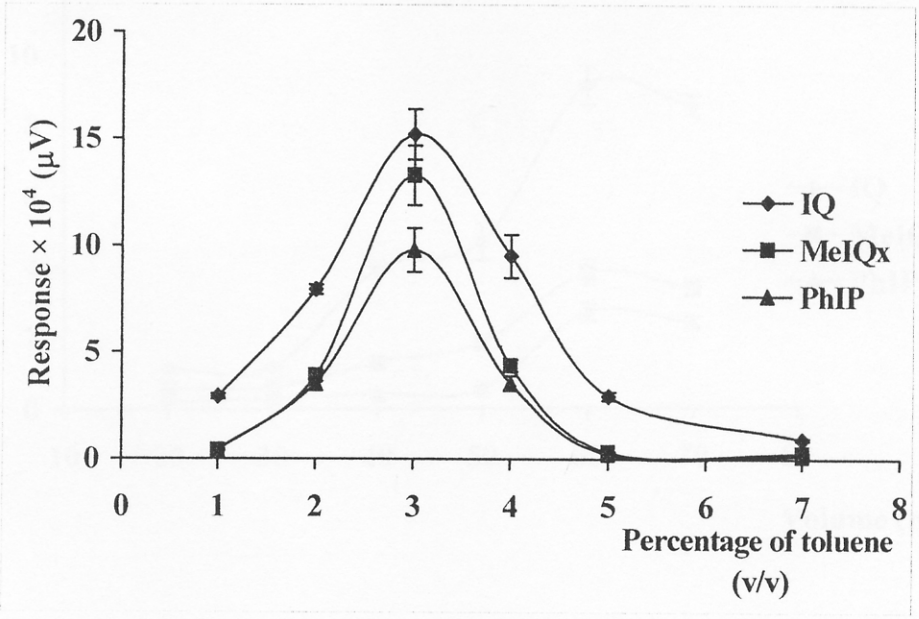

Figure 52 Responses using various amount of toluene in mixed solvents

Table 44 Responses using various amount of eluting solvents

Volume of 3% toluene + dichloromethane (mL)	Response* × 10^4 (μV) ± SD		
	IQ	MeIQx	PhIP
20	1.1 ± 0.1	0.60 ± 0.01	0.23 ± 0.01
30	1.2 ± 0.1	0.60 ±0.04	0.30 ± 0.01
40	3.9 ± 0.2	1.30 ± 0.06	0.42 ± 0.03
50	4.7 ± 0.5	1.90 ± 0.05	0.6 ± 0.1
60	9.1 ± 0.6	3.8 ± 0.4	2.7 ± 0.3
70	8.5 ± 0.3	3.4 ± 0.2	2.4 ± 0.2

*5 replications, RSD ≤ 10%

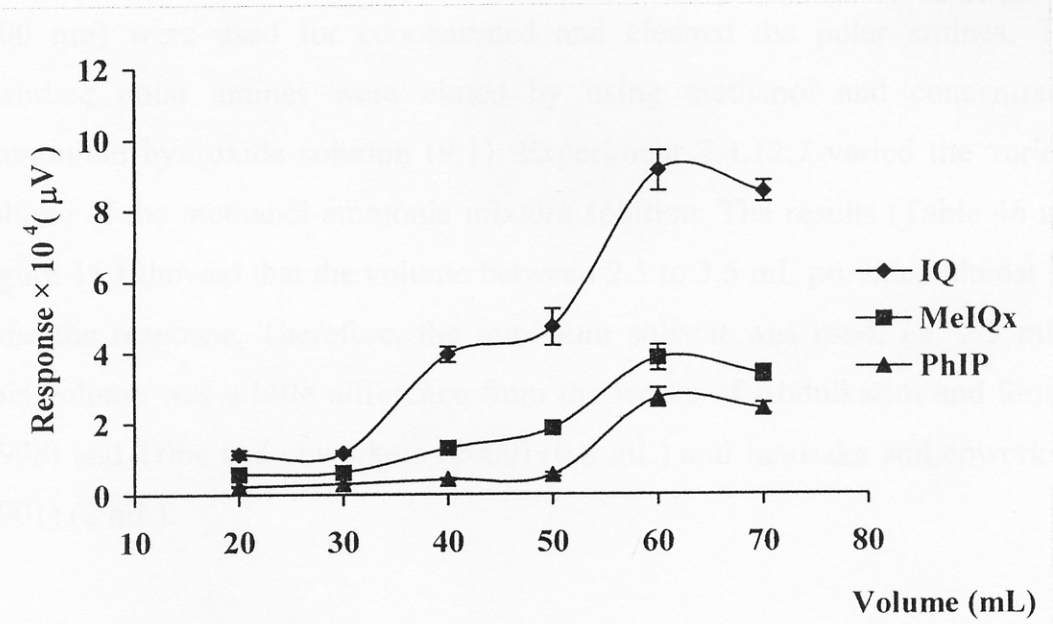

Figure 53 Responses using various amounts of eluting solvents

3.5.6 Amount of 0.5 *M* ammonium acetate, pH 8.0

Ammonium acetate, 0.5 *M* pH 8.0 was used in the elution process of HCAs which were bonded on the PRS cartridges. Therefore, the amount of ammonium acetate was an importance parameter because it would affected the extraction efficiency. If it is too small it may not be sufficient to elute the analytes on the PRS cartridges. Experiment 2.4.12.6 varied the volume of 0.5 *M* ammonium acetate, pH 8.0 and the results (Table 45 and Figure 54) showed that the response of 25 to 30 mL were high with not much difference. Therefore, to minimize the amount of ammonium acetate a 25 mL was selected to be the appropriate volume to elute HCAs from PRS cartridges.

3.5.7 Amount of methanol: ammonia solution mixture (9:1, v/ v)

In this study the chemically bonded phase C_{18} cartridges (100 mg) were used for concentrated and cleaned the polar amines. The adsorbed polar amines were eluted by using methanol and concentrated ammonium hydroxide solution (9:1). Experiment 2.4.12.7 varied the various volume of the methanol-ammonia mixture solution. The results (Table 46 and Figure 55) showed that the volume between 2.5 to 3.5 mL provided almost the same the response. Therefore, the minimum solvent was used, *i.e.* 2.5 mL . This volume was a little difference from the works of Abdulkarim and Smith, (1998) and Tribe and coworkers (2000) (0.8 mL) and Janoszka and coworkers (2001) (2 mL).

Table 45 Responses using various amounts of 0.5 *M* ammonium acetate, pH 8.0

Volume of 0.5 *M* ammomium acetate pH 8	Response* × 10^4 (μV) ± SD		
	IQ	MeIQx	PhIP
15	12.8 ± 1.1	3.6 ± 0.4	1.1 ± 0.1
20	17.4 ± 1.0	5.6 ± 0.6	1.5 ± 0.1
25	25.1 ± 2.8	11.6 ± 1.0	3.3 ± 0.3
30	24.9 ± 2.0	11.8 ± 1.0	3.6 ± 0.4

*5 replications, RSD ≤ 10 %

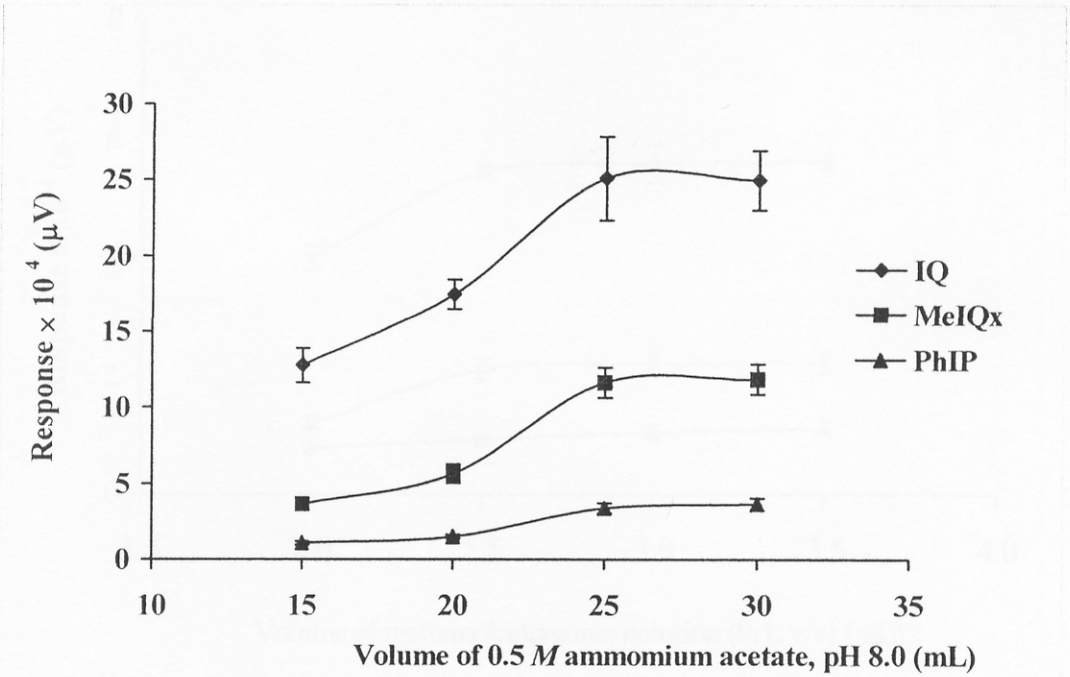

Figure 54 Responses using various amounts of 0.5 *M* ammonium acetate, pH 8.0

Table 46 Responses using various amounts of methanol: ammonia solution (9:1, v/ v)

Volume of methanol: ammonia solution mixture (9:1, v/ v)	Response* × 10^4 (μV) ± SD		
	IQ	MeIQ	PhIP
2.0	4.0 ± 0.2	1.2 ± 0.1	0.8 ± 0.1
2.5	5.4 ± 0.1	2.1 ± 0.2	0.9 ± 0.1
3.0	5.6 ± 0.3	2.2 ± 0.2	1.0 ± 0.1
3.5	5.6 ± 0.1	2.2 ± 0.2	1.1 ± 0.1

*5 replications, RSD ≤ 10%

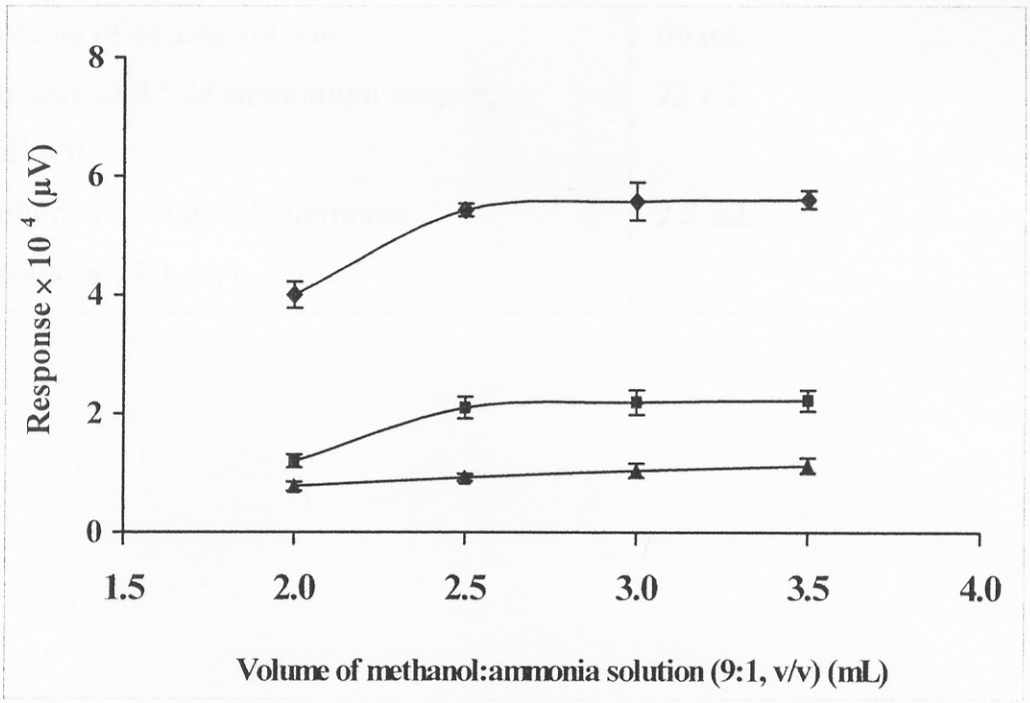

Figure 55 Responses using various amounts of methanol: ammonia solution (9:1, v/ v)

The optimum conditions of the sample preparation procedure for the analysis of heterocyclic amines in food with GC-NPD using HP-5 capillary column are summarized in Table 47. The chromatograms obtained using these optimum conditions is shown in Figure 56. The results obtained by these sample preparation steps showed no interferences, gave high extraction efficiency and base line resolution.

Table 47 Optimum conditions of sample preparation

Parameters	Optimum values
Extraction time by ultrasonic extraction	2 hours
Flow rate of eluting solvent	2 mL min^{-1}
Type of eluent solvent	dichloromethane + toluene
Percentage of toluene	3% (v/v)
Volume of eluting solvent	60 mL
Volume of 0.5 *M* ammonium acetate, pH 8.0	25 mL
Volume of methanol: ammonia solution (9:1,v/v)	2.5 mL

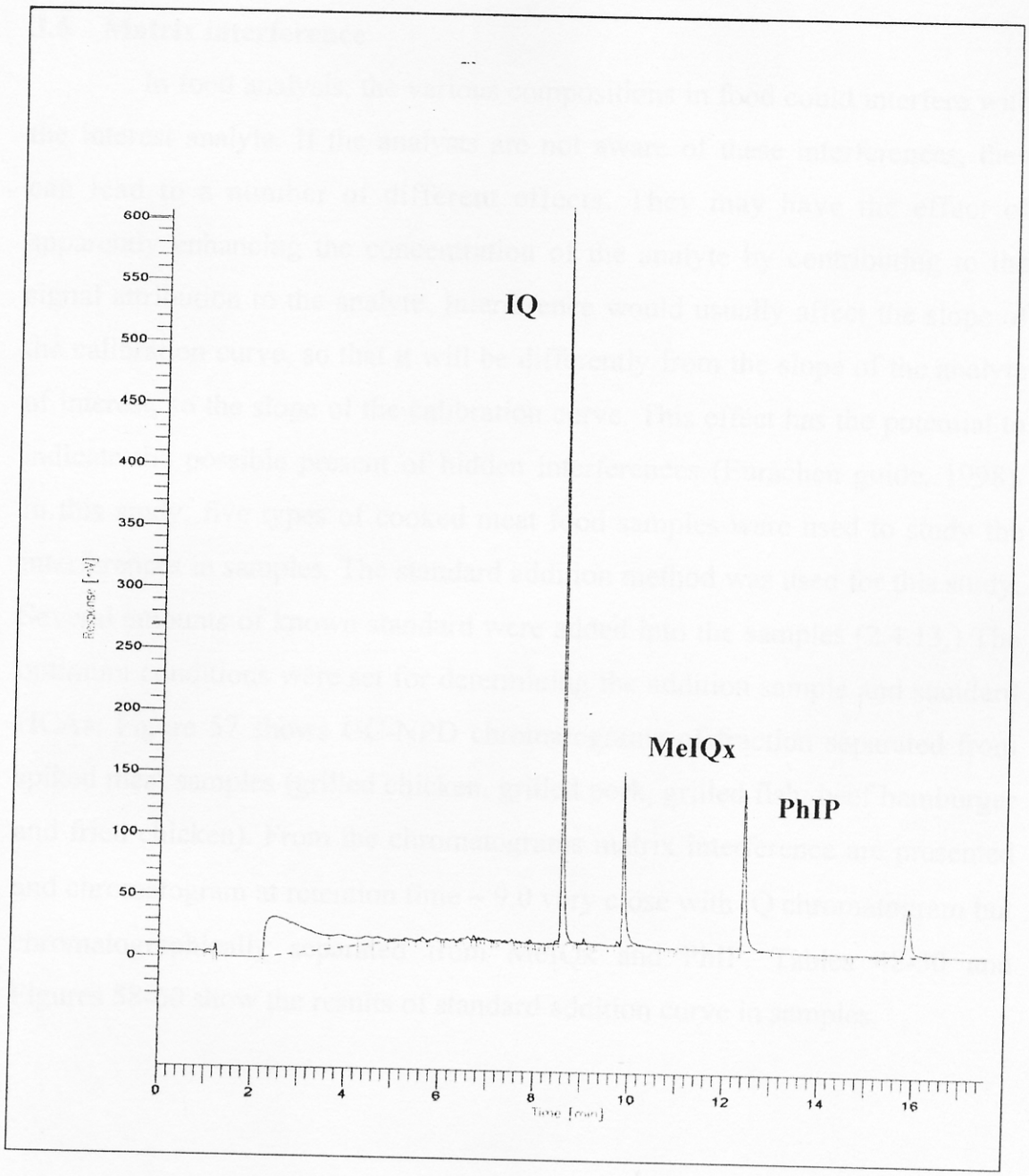

Figure 56 GC–NPD chromatograms HCAs fraction isolated from spiked meat sample at optimum condition of sample preparation

3.6 Matrix interference

In food analysis, the various compositions in food could interfere with the interest analyte. If the analysts are not aware of these interferences, they can lead to a number of different effects. They may have the effect of apparently enhancing the concentration of the analyte by contributing to the signal attribution to the analyte. Interference would usually affect the slope of the calibration curve, so that it will be differently from the slope of the analyte of interest, so the slope of the calibration curve. This effect has the potential to indicate the possible present of hidden interferences (Eurachen guide, 1998). In this study, five types of cooked meat food samples were used to study the interferences in samples. The standard addition method was used for this study. Several amounts of known standard were added into the samples (2.4.13.) The optimum conditions were set for determining the addition sample and standard HCAs. Figure 57 shows GC-NPD chromatograms of fraction separated from spiked meat samples (grilled chicken, grilled pork, grilled fish, beef hamburger and fried chicken). From the chromatograms matrix interference are presented and chromatogram at retention time ~ 9.0 very close with IQ chromatogram but chromatographically separated from MeIQx and PhIP. Tables 48-50 and Figures 58-60 show the results of standard addition curve in samples.

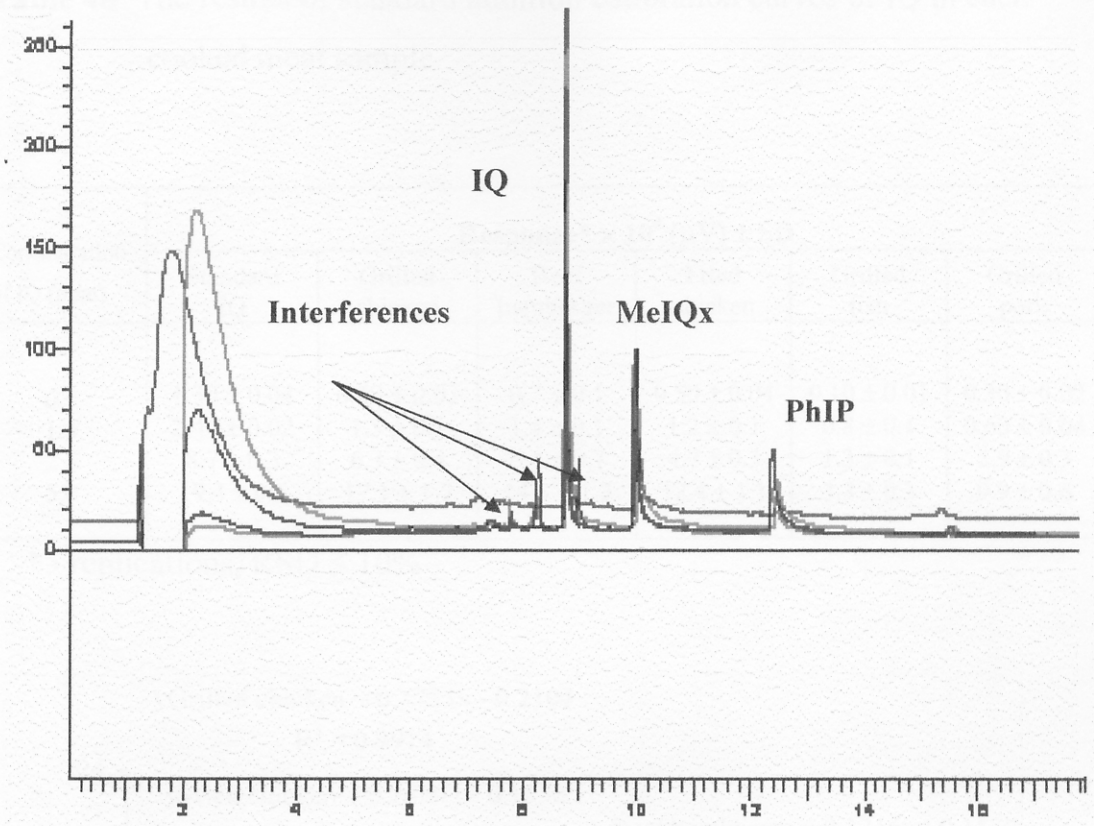

Figure 57 GC-NPD chromatograms of HCAs of fraction separated from spiked in meat samples

Table 48 The results of standard addition calibration curves of IQ in each cooked meat sample

Concentration of IQ (ppm)	Response* × 10^4 (μV) ± SD					
	Standard IQ	Grilled chicken	Beef hamburger	Fried chicken	Grilled fish	Grilled pork
0.5	1.30 ± 0.04	0.40 ± 0.03	0.7 ± 0.1	0.50 ± 0.04	0.10 ± 0.01	0.30 ± 0.02
1.0	2.40 ± 0.02	1.5 ± 0.1	1.4 ± 0.1	1.2 ± 0.1	0.8 ± 0.1	0.60 ± 0.04
2.5	8.7 ± 0.3	6.3 ± 0.4	6.4 ± 0.7	4.7 ± 0.3	1.3 ± 0.1	3.9 ± 0.3
5.0	19.4 ± 0.5	17.1 ± 1.7	14.8 ± 1.3	12.4 ± 1.1	3.3 ± 0.3	9.9 ± 0.6

*5 replications, RSD ≤ 10%

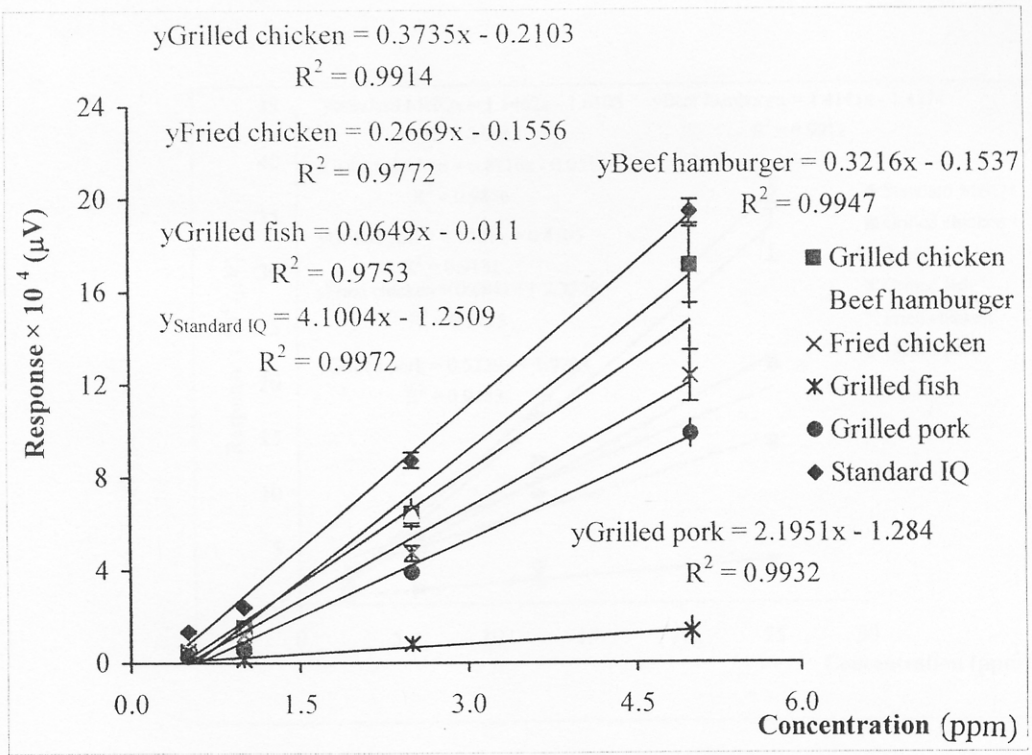

Figure 58 The results of standard addition calibration curves of IQ in each cooked meat sample

Table 49 The results of standard addition calibration curves of MeIQx in each cooked meat sample

Concentration of MeIQx (ppm)	Response* × 10^4 (μV) ± SD					
	Standard MeIQx	Grilled chicken	Beef hamburger	Fried chicken	Grilled fish	Grilled pork
2.5	1.5 ± 0.1	1.6 ± 0.1	1.1 ± 0.1	3.5 ± 0.2	0.40 ± 0.04	2.0 ± 0.1
6.25	9.3 ± 0.2	5.1 ± 0.4	7.3 ± 0.6	6.3 ± 0.5	1.3 ± 0.1	5.9 ± 0.6
12.5	17.1 ± 1.1	12.7 ± 0.6	18.1 ± 2.0	12.5 ± 0.9	2.7 ± 0.1	9.8 ± 1.0
25.0	37.1 ± 1.4	21.6 ± 2.3	33.1 ± 2.9	18.8 ± 1.6	3.6 ± 0.4	14.3 ± 1.2

*5 replications, RSD ≤ 10%

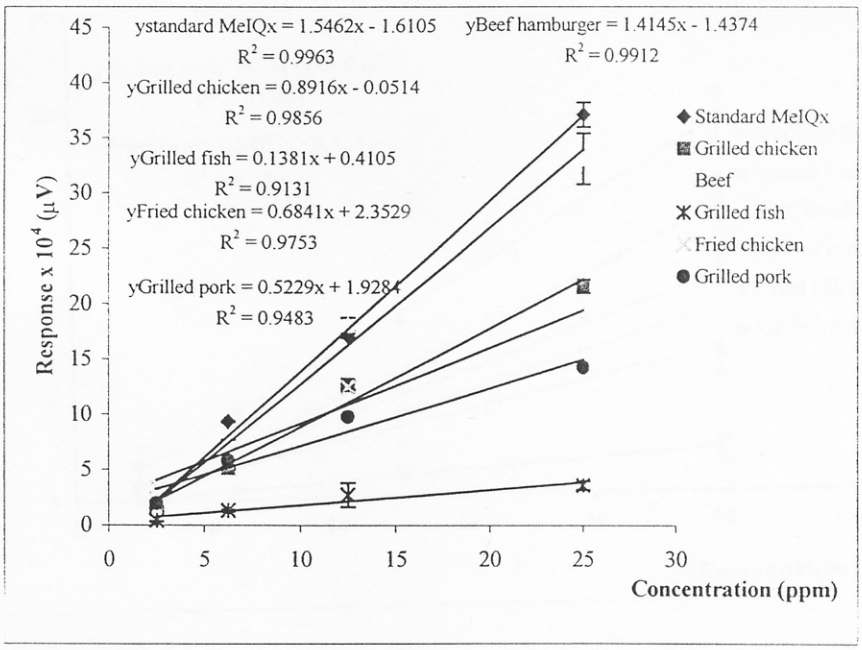

Figure 59 The results of standard addition calibration curves of MeIQx in each cooked meat sample

Table 50 The result of standard addition calibration curves of PhIP in each cooked meat sample

Concentration Of PhIP (ppm)	Response * $\times 10^4$ (μV) ± SD					
	Standard PhIP	Grilled Chicken	Beef hamburger	Fried chicken	Grilled Fish	Grilled pork
5.0	1.5 ± 0.04	0.7 ± 0.1	0.40 ± 0.03	0.10 ± 0.01	0.12 ± 0.01	0.30 ± 0.03
12.5	2.1 ± 0.03	2.5 ± 0.2	1.9 ± 0.1	0.5 ± 0.1	1.9 ± 0.21	2.3 ± 0.1
25.0	7.7 ± 0.2	5.8 ± 0.4	3.5 ± 0.4	1.2 ± 0.1	4.3 ± 0.3	5.1 ± 0.3
50.0	19.4 ± 0.8	15.0 ± 1.1	9.8 ± 0.7	2.2 ± 0.2	7.1 ± 0.6	11.3 ± 1.1

*5 replications, RSD ≤ 10%

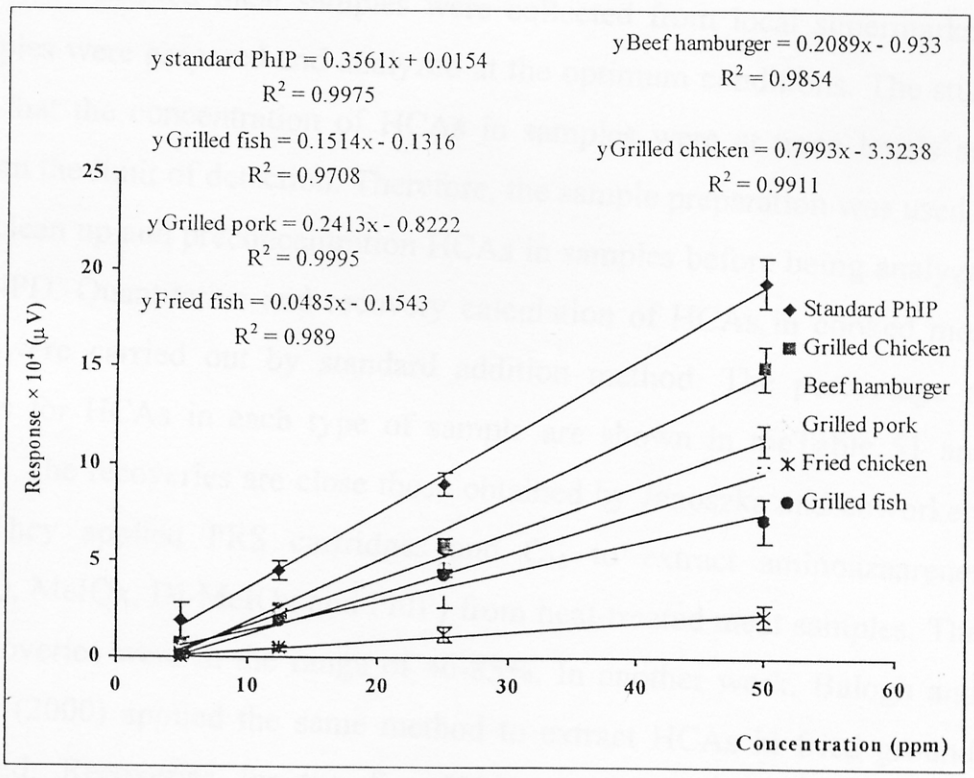

Figure 60 The results of standard addition calibration curves of PhIP in each cooked meat sample

3.7 Qualitative and quantitative analysis of HCAs in cooked meat samples

3.7.1 Qualitative analysis

The optimum conditions of GC-NPD were used to analyse HCAs in food samples. For qualitative analysis, the retention time, t_R were used. The average t_R of IQ, MeIQx and PhIP derivatives were 8.60, 9.92 and 12.54 minutes respectively.

3.7.2. Recovery and Quantitative Analysis

Cooked meat samples were collected from local supermarkets. All samples were prepared and analyzed at the optimum conditions. The study showed that the concentration of HCAs in samples were at trace levels and lower than the limit of detection. Therefore, the sample preparation was used to extract, clean up and preconcentration HCAs in samples before being analyzed by GC-NPD. Quantitative and recovery calculation of HCAs in cooked meat samples were carried out by standard addition method. The percentage of recoveries for HCAs in each type of sample are shown in theTable 51 and Figure 61. The recoveries are close those obtained by Janoszka and coworkers (2001). They applied PRS cartridges and C_{18} to extract aminoazaarenes (IQ, MeIQ, MeIQx, Di-MeIQx and PhIP) from heat-treated meat samples. The HCAs recoveries were in the range of 46-85%. In another work, Balogh and coworkers (2000) applied the same method to extract HCAs in fried ground beef pattied. Recoveries for the five HCAs were as follows:IQ 58.2%, MeIQ 51.7%, MeIQx 66.7%, DiMeIQx 72.1% and PhIP 32.1%.

Table 51 The percentage of recoveries of the three HCAs in cooked meat samples

Types of samples	% Recovery ± SD		
	%IQ	%MeIQx	%PhIP
Grilled chicken	84.8± 7.2	63.1 ± 6.4	83.3 ± 6.0
Grilled pig	63.1 ± 5.9	46.0 ± 4.6	58.6 ± 4.7
Baker beef	89.0 ± 8.4	36.3 ± 3.0	33.9 ± 3.1
Fried chicken	90.0 ± 7.0	47.4 ± 4.2	48.1 ± 3.4
Grilled fish	55.1 ± 5.5	42.8 ± 3.8	33.2 ± 3.3

*5 replications, RSD ≤ 10%

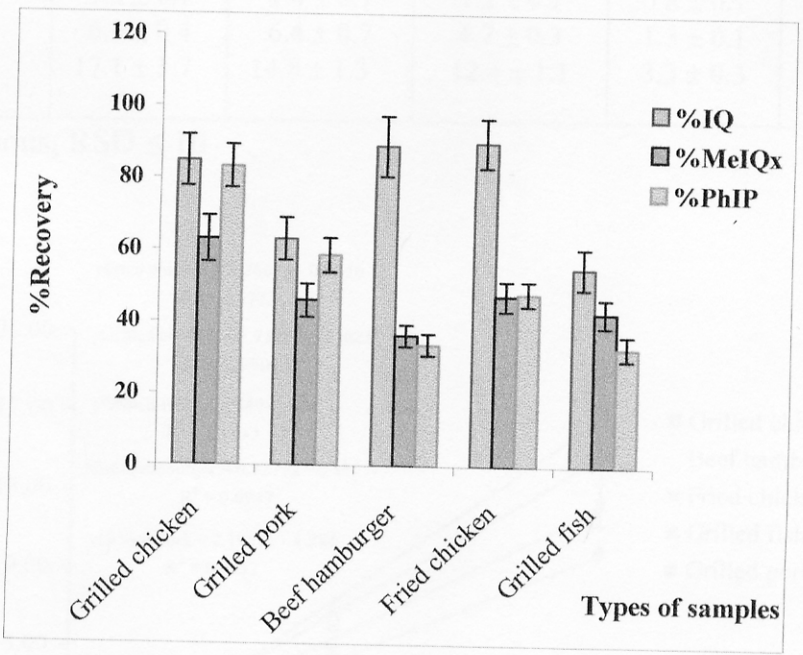

Figure 61 The percentage of recoveries of the three HCAs in cooked meat samples

The concentration of IQ, MeIQx and PhIP in all cooked meat samples were not detected by external standard addition method, it is possible that the amount of IQ, MeIQx and PhIP lower that the limit of detection. The confirmation was carried out by standard addition method. The results are shown in Table 52-55 and Figure 62-64

Table 52 The results of standard addition calibration curves of IQ in each cooked meat sample

Concentration of IQ ($\mu g\ g^{-1}$)	Response* $\times 10^4$ (μV) $\pm$ SD				
	Grilled chicken	Beef hamburger	Fried chicken	Grilled fish	Grilled pork
0.5	0.40 $\pm$ 0.03	0.7 $\pm$ 0.1	0.50 $\pm$ 0.04	0.10 $\pm$ 0.01	0.30 $\pm$ 0.02
1.0	1.5 $\pm$ 0.1	1.4 $\pm$ 0.1	1.2 $\pm$ 0.1	0.8 $\pm$ 0.1	0.60 $\pm$ 0.04
2.5	6.3 $\pm$ 0.4	6.4 $\pm$ 0.7	4.7 $\pm$ 0.3	1.3 $\pm$ 0.1	3.9 $\pm$ 0.3
5.0	17.1 $\pm$ 1.7	14.8 $\pm$ 1.3	12.4 $\pm$ 1.1	3.3 $\pm$ 0.3	9.9 $\pm$ 0.6

*5 replications, RSD $\leq$ 10

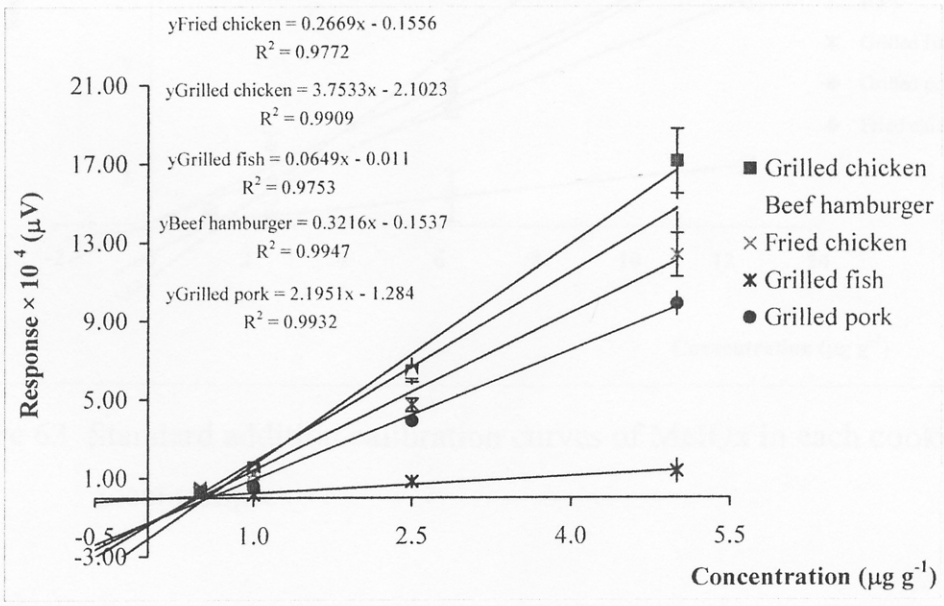

Figure 62 Standard addition calibration curves of IQ in each cooked meat sample

Table 53 The results of standard addition calibration curves of MeIQx in each cooked meat sample

Concentration of MeIQx ($\mu g\ g^{-1}$)	Response* $\times 10^4$ (μV) ± SD				
	Grilled chicken	Beef hamburger	Fried chicken	Grilled fish	Grilled pork
1.25	0.30 ± 0.02	0.50 ± 0.04	0.60 ± 0.04	0.10 ± 0.01	0.8 ± 0.1
2.5	1.6 ± 0.1	1.1 ± 0.1	3.5 ± 0.2	0.40 ± 0.04	2.0 ± 0.1
6.25	5.1 ± 0.4	7.3 ± 0.6	6.3 ± 0.5	1.3 ± 0.1	5.9 ± 0.6
12.5	12.7 ± 0.6	18.1 ± 2.0	12.5 ± 0.9	2.7 ± 0.1	9.8 ± 1.0

*5 replications, RSD ≤ 10

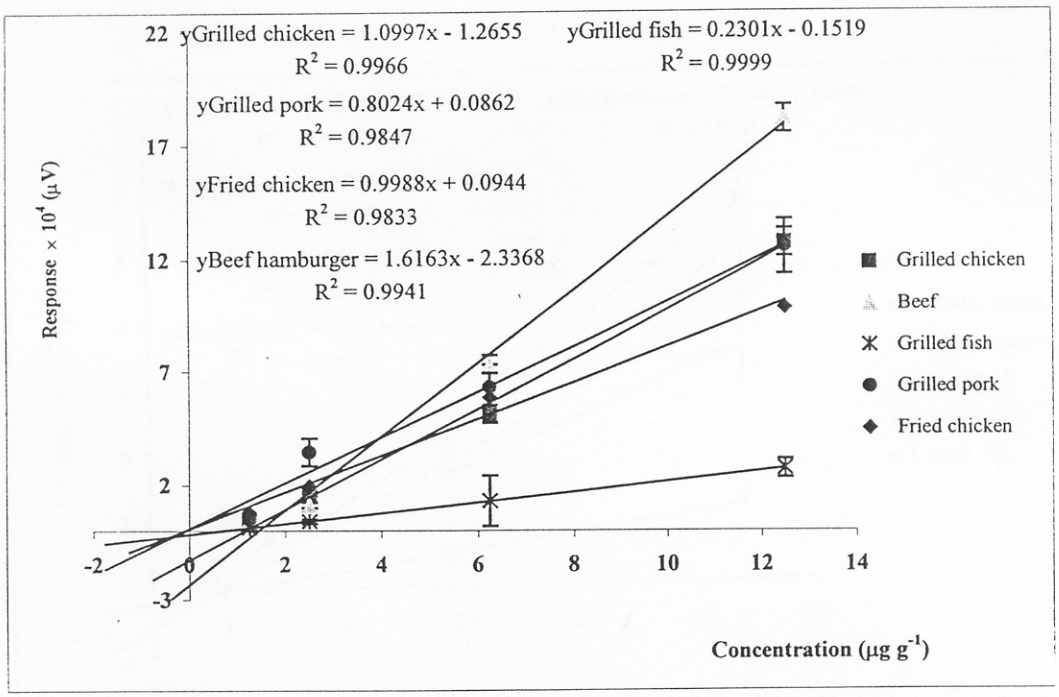

Figure 63 Standard addition calibration curves of MeIQx in each cooked meat sample

Table 54 The results of standard addition calibration curves of PhIP in each cooked meat sample

Concentration Of PhIP ($\mu g\ g^{-1}$)	Response * $\times 10^4$ (μV) ± SD				
	Grilled Chicken	Beef hamburger	Fried chicken	Grilled Fish	Grilled pork
2.5	0.20 ± 0.01	0.20 ± 0.01	0.020 ± 0.003	0.050 ± 0.004	0.20 ± 0.02
5.0	0.7 ± 0.1	0.40 ± 0.03	0.10 ± 0.01	0.12 ± 0.01	0.30 ± 0.03
12.5	2.5 ± 0.2	1.9 ± 0.1	0.5 ± 0.1	1.9 ± 0.2	2.3 ± 0.1
25.0	5.8 ± 0.4	3.5 ± 0.4	1.2 ± 0.1	4.3 ± 0.3	5.1 ± 0.3

*5 replications, RSD ≤ 10

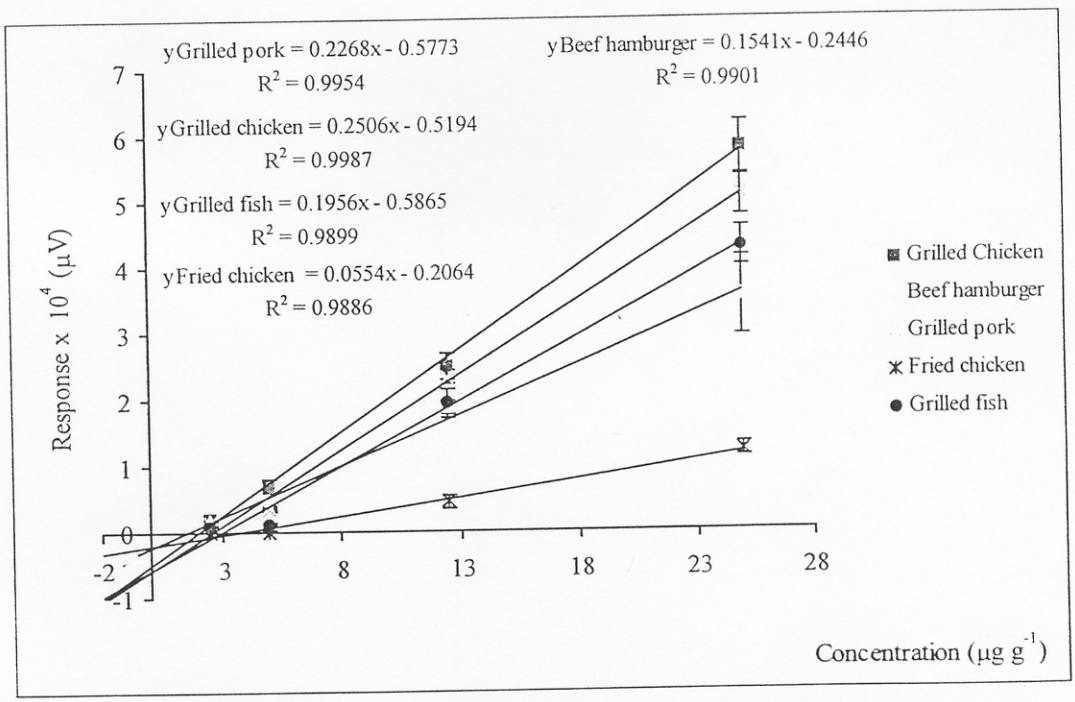

Figure 64 Standard addition calibration curves of PhIP in each cooked meat sample

Table 55 The HCAs concentrations of samples determined by standard addition method

Types of sample	Amount of HCAs (μg g^{-1})		
	IQ	MeIQx	PhIP
Grilled pork	n.d	0.11	n.d
Grilled chicken	n.d	n.d	n.d
Grilled fish	n.d	n.d	n.d
Beef hamburger	n.d	n.d	n.d
Fried chicken	n.d	0.09	n.d

* n.d = non detectectable